How Topography Influences the Fate of Human Neural Progenitor Cells

Studying cellular mechanoresponses and mechanotransduction using cell cultures on electrospun fibrous scaffolds

by

Jacob Karlström

Lund University

September 24, 2020

A thesis submitted for the degree of *Master of Science in Engineering Nanoscience* at the *Faculty of Engineering at Lund University.*

Subject: Applied Biochemistry (KBKM05)
Division: Dept Clinical Sciences, Lund University | Dept. Biology, Lund University
Supervisor: Ulrica Englund Johansson, Assoc. Prof, Dept. Clinical Sciences, Lund University
Examiner: Lei Ye, Professor, Dept. Pure and Applied Biochemistry, Lund University
Student Opponent: Hampus Ekström, Faculty of Engineering, Lund University

Acknowledgements

I wish to express my gratitude to my supervisor **Ulrica Englund-Johansson** for important advice and fruitful discussions; **Andreas Boross** for our collaboration with cell culture; **Karl Westerlund** for introduction to many of the experimental techniques used; **Carl-Johan Hörberg** for introduction to cell culture; **Hodan Abdshill** for general help and technical assistance in the lab; **Fredrik Johansson** for helpful advice as well as assistance with scanning electron microscopy; **Cellevate AB** for sponsoring of electrospun fibrous scaffolds and for technical advice; **Marina Castro Zalis** for many of the protocols used for the experimental work of this thesis; and **Panajot Kristofori** for input on the written report and oral presentation.

Jacob Karlström
September 2020

Abstract

Novel biomimetic three-dimensional scaffolds have emerged over the last decades, and are promising for applications in regenerative therapies, as well as in *in vitro* disease modelling and drug testing. Thanks to their added dimension, these scaffolds are able to more accurately mimic the topography of native cellular microenvironments compared to traditionally used two-dimensional culture substrates. Here we cultured human neural progenitor cells on electrospun fibrous scaffolds in order to investigate how the fibrous topographical landscape influences differentiation capacity and phenotypic fate. In contrast to previous findings, we found that differentiation of progenitor cells cultured on fibrous scaffolds does not differ significantly from that of progenitors cultured on flat glass slides. However, we found that the substrate has a significant effect on the morphology and alignment of cell nuclei. To examine mechanotransductory pathways responsible for interpreting topographical cues into cell responses we cultured cells with the myosin II inhibitor blebbistatin. As there were no differences in differentiation between cells cultured on fibrous scaffolds or glass slides, we could not elucidate any mechanotransductory pathways. Nevertheless, we found that myosin II inhibition led to altered cell and nucleus morphology. Finally, we highlight the need for more consistent methods and continued research on this topic.

Acronyms

2D two-dimensional
3D three-dimensional
ANOVA analysis of variance
BSA bovine serum albumin
CNS central nervous system
DAPI 4′,6-diamidino-2-phenylindole
DIV days *in vitro*
DMEM Dulbecco's Modified Eagle Medium
DMSO dimethyl sulphoxide
ECM extracellular matrix
F12 Ham's F12 nutrient mixture
FBS fetal bovine serum
GFAP glial acidic fibrially protein
hbFGF human basic fibroblast growth factor
hEGF human epidermal growth factor
hLIF human leukaemia inhibitory factor
hNPCs human neural progenitor cells
IAC integrin-associated complex
ICC immunocytochemistry
MAP2 microtubule associated protein 2
MSCs mesenchymal stem cells
NSCs neural stem cells
PBS phosphate-buffered saline
PCL polycaprolactone
PFA paraformaldehyde
PLL poly-L-lysine
PLLA poly-L-lactic acid
PNS peripheral nervous system
RT room temperature
SEM standard error of the mean
SOX2 sex determining region Y-box 2
βIIIT class III β-tubulin

Contents

Chapter 1

Introduction

This thesis aims to improve our understanding of how nanotopography affects neural progenitor cell behaviour. This is important in the context of neurological disorders where three-dimensional (3D) scaffolds have great potential for use in neuroregenerative therapies, e.g. in cell transplantation, and *in vitro* modelling. For these applications, control over cell behaviour is vital for both successful tissue regeneration as well accurate modelling of native microenvironments. Thus, designing scaffolds with suitable mechanical properties is of great importance.

In this thesis, human neural progenitor cells (hNPCs) were cultured on electrospun fibrous scaffolds and their behaviour was compared with that of hNPCs grown on traditionally used flat substrates. Furthermore, the effects of myosin II inhibition on hNPCs were studied to elucidate pathways responsible for translating mechanical cues into a cellular response. This introductory chapter serves to introduce the reader to relevant background theory.

1.1 NEUROLOGICAL DISORDERS AND THE NEED FOR NEW THERAPIES

Neurological disorders are indisputably a source of great suffering for hundreds of millions of people all over the globe; not only do they reduce life expectancy and quality of life for the person affected, but also place a huge burden on family and caregivers, and impose large costs on society. For many neurological disorders, we still have a poor understanding of their cause, and despite enormous amounts of research, we have yet to find cures.

Neurodegenerative diseases—a subset of neurological disorders—are characterized by loss of neural cells in the central nervous system (CNS), or in the peripheral nervous system (PNS), and include diseases such as Alzheimer's, Parkinson's, multiple sclerosis and amyotrophic lateral sclerosis. These diseases have wide arrays of symptoms, ranging from cognitive impairment to paralysis and death. Due to the limited regenerative capacity of the CNS (*1*) and the lack of effective pharmaceutical treatments, the progression of neurodegenerative diseases can currently only be slowed down, but the damage can not be reversed. In order to finally beat these diseases, breakthroughs are needed in disease research, drug development and regenerative strategies.

In Vitro Models for Disease Modelling and Drug Development

In vitro models are essential for disease research and drug development. They provide means of studying disease mechanics and testing drug candidates in controlled environments, and in contrast to animal models, human cell lines can be used. However, traditional two-dimensional (2D) cell culture systems such as glass petri dishes—which have been the predominant *in vitro* models for over a century—are poor mimics of native microenvironments, failing to recapitulate important characteristics such as 3D topography, cell interaction with the extracellular matrix (ECM), and mechanical properties. This leads to unnatural cell morphology and behaviour, and consequently produces results which may not be reproducible *in vivo* (*2–4*).

In order to enable more progress in finding cures and treatments for neurological diseases, improved *in vitro* models are essential. Over the last decades, several different types of novel culture models have emerged which aim to better simulate the native 3D microenvironment. Three of the more prominent ones are electrospun fibrous scaffolds, hydrogel scaffolds and scaffolds made from decellularized ECM. When cultured in these scaffolds, cells are no longer spatially restricted by the horizontal plane, and can experience more natural interactions with the substrate as well as with other cells, thus allowing more *in vivo*-like behaviour (*5*).

Neuroregenerative Therapies

Artificial scaffolds are also promising for use in neuroregenerative therapies in the CNS—therapies which can replace or regenerate cells damaged or lost due to neurodegenerative diseases or traumatic injury. Two main approaches are being researched for neuroregeneration: drug- or biopharmaceutical-based strategies and cell-based strategies (*6*). The former aims to deliver bioactive molecules to the CNS to promote tissue regeneration, while the latter uses cell transplants to replace cells or promote neurogenesis via secretion of various factors (*6*). Cell-based therapeutic strategies have been used in clinical trials, e.g. for transplantation of stem cells into stroke patients (*7*). However, positive effects have been limited, with low cell survival and poor integration observed in the region (*6*). These problems partly stem from the hostile environment at the site of the damage, which is a result of the intrinsic response to neural atrophy.

After traumatic injury, stroke, or as a result of neurodegenerative diseases, neural cells die by several different mechanisms. The accumulation of toxic debris from these cells activates a response from nearby immune cells which eventually leads scar formation around the affected region, effectively turning it into a cavity. While this process certainly is a beneficial measure from a protective standpoint, the sealed off cavity is rendered an inhibitory environment for neuroregeneration (*8*). This is part of the reason behind poor intrinsic neuroregeneration in the CNS, and is an obstacle that needs to be overcome by cell-based neuroregenerative strategies. Transplantation

of scaffolds is a promising novel strategy providing the needed structure for tissue regeneration in such a cavity, and has been successfully performed on animals (*9*, *10*).

1.2 MIMICKING THE CELLULAR MICROENVIRONMENT

In vitro models for disease research and drug development must accurately simulate the relevant *in vivo* microenvironment in order to provide reliable and translatable results. For regenerative therapies, a growth-permissive microenvironment must be engineered in order to promote tissue regeneration. Both of these challenges require knowledge of native cellular microenvironments and what important cues they provide which guide cell behaviour. The cellular microenvironment can be divided into *biochemical* and *mechanical* cues. One of the key elements of the microenvironment is the ECM, a 3D network of macromolecules (see Box 1.1) which surrounds cells and provides structure and important cues (*11*).

The Biochemical Microenvironment

The chemical environment surrounding a cell *in vivo* is very complex and changes throughout life, from development to adulthood, and as a result of disease. Not only are soluble nutrients and factors needed for cell survival and normal function, but many chemical cues also control the fate of stem and progenitor cells (*6*). For example, neurotrophic factors, such as nerve growth factor or glial cell derived neurotrophic factors, have roles in regulation of survival, proliferation and maturation of certain neuronal types (*12*).

The ECM also provides important biochemical signals in the form of proteins which are detected by cellular receptors. The presence or absence of ECM proteins—such as fibronectins, laminins and collagens—have been shown to influence differentiation of stem cells (*13*). For example, Rowlands et al. (*14*) showed that differentiation fate of human mesenchymal stem cells (MSCs)—a type of pluripotent stem cells found in bone marrow—cultured *in vitro* was affected by protein coating of the substrate. Furthermore, different artificial peptides derived from ECM proteins have been shown to influence neural cell processes (*6*). For instance, the fibronectin-derived sequence Arg-Gly-Asp increases cell adhesion and cell viability (*15*), while the laminin-derived sequence Ile-Lys-Val-Ala-Val promotes neurite outgrowth (*16*).

The cellular proteins which detect these ECM proteins are the *integrins*—a family of transmembrane receptors responsible for adhesion and transmembrane signal transduction (*17*). Integrins are heterodimers of an α and β subunit. Various combinations of different types α and β subunits yield integrins with specific affinities for different extracellular ligands. (*18*). In addition to their role in chemical signalling, integrins are also vital for cellular mechanosensation, a topic which I kindly refer the reader to further explore in Section 1.3.

Box 1.1: Major CNS ECM Constituents

Proteoglycans are glycoproteins which are covalently linked to sulphated glycosaminoglycan sidechains. Due to the anionic nature of these sidechains, they are able to efficiently bind water and cations.
Hyaluronan consists of single chains of non-sulphated glycosaminoglycans. These too are of anionic nature and can bind massive amounts of water, making them a gel-like substance.
Tenascins are large glycoproteins which exist as different types. These types have either adhesive or anti-adhesive properties and are believed to have a role in guiding axonal growth.
Fibronectins are large glycoproteins widely present in the ECM of the developing CNS. They contain domains which bind to other fibronectins, other ECM components or cellular receptors. Like tenascins, fibronectins are believed to have a role in axonal growth as well as neuronal migration.
Laminins are large glycoproteins which are present in the CNS in several different heterotrimeric forms. Laminins are important for adhesion and growth of both developing and mature neurons. (*11*, *19–21*)

Mechanical Factors

For a long time, chemical signals were considered the main determinants of cell behaviour and stem cell differentiation. However, more recent research has highlighted the importance the mechanical environment for control of cell fate (*13*). Two important properties of the mechanical environment are substrate stiffness and topography.

Substrate stiffness has been shown to have a significant impact on differentiation and proliferation of stem cells. For example, Engler et al. (*22*) showed the importance of substrate stiffness by culturing MSCs on substrates with different stiffnesses; they showed that MSCs cultured on softer matrices with elasticities mimicking those of brains ($E \sim 0.1$ kPa to 1 kPa) promoted neuronal fate, while more rigid matrices proved myogenic or osteogenic. Leipzig and Shoichet (*23*) further signified the importance of stiffness for neural differentiation; in their study they showed that softer hydrogels ($E < 1$ kPa) promoted neuronal differentiation of neural stem/progenitor cells, while stiffer hydrogels ($E > 7$ kPa) favoured oligodendrocytal differentiation.

The topographical landscape of the ECM is technically challenging to characterize *in vivo*, and important parameters, such as fibre diameters and pore sizes vary both between and within tissue (*24*). However, several different topographical cues with implications in cell behaviour have been studied *in vitro*. For example, aligned electrospun fibres have been shown to promote neuronal differentiation and affect neurite direction and elongation of neural stem cells (NSCs) (*25*, *26*). Many other geometrical features, among them microgrooves and patterned-islands, have also been shown to affect a multitude of cell behaviours (*27–29*). How stiffness and topography are converted into a cellular response is further discussed in Section 1.3.

1.3 MECHANOTRANSDUCTION

Mechanotransduction refers to a collection of mechanisms used by cells to sense their mechanical environment. Different strategies are used for this purpose and involve mechanosensitive ion-channels, cell-cell adhesions, and cell-ECM adhesions (*30*). The latter of these is perhaps the most important and is the focus of this thesis.

Mechanotransduction involves many different proteins and complex pathways—many of which are still poorly understood and may vary between cell types (*30*, *31*). Among the key players of cell-ECM mechanosensation are integrins. These transmembrane proteins form the core of integrin-associated complexes (IACs) via which cells bind to the ECM. The composition of these complexes is indeed complex and includes a multitude of different molecules with various functions: some molecules, e.g. vinculin and talin, are responsible for connection between integrins and actin filaments, while others, e.g. focal adhesion kinase and paxillin, have signalling or regulatory roles (*32*).

Integrin-ECM binding alone does not provide the cell with mechanical information; to sense the mechanical environment, force needs to be applied on the IACs. For sensing the rigidity of the environment this force stems from actomyosin contraction: actin polymerization at nascent cell edges pushes the cell membrane outward while myosin II contraction pulls actin inwards; this leads to a cyclic net movement of actin in the cell. Since IACs bind to actin via adaptor proteins, a cyclic force is applied on the IACs and the adaptor proteins. Although a complete understanding of the transduction from mechanical to chemical signals is lacking, one of the mechanisms which has been observed is that force changes the conformation of talin, exposing new binding sites for vinculin, which in turn leads to a cascade of signalling events (*30*, *31*, *33*).

The forces which are generated by actomyosin contraction are not limited to IACs at the cell membrane, but are furthermore transmitted via the cytoskeleton to the cell nucleus (*34*). Here the mechanical forces affect the nucleus morphology which in turn may affect gene expression (*35*).

Disruption of Mechanotransductory Pathways Using Blebbistatin as a Myosin II Inhibitor

Blebbistatin is a small molecule with inhibitory effects on muscle and non-muscle Myosin II function (*36*). As mentioned, actomyosin contraction is used mechanotransduction and thus blebbistatin can be used to determine if myosin-dependent steps are involved in different phenomena. As an example, blebbistatin was used in the previously mentioned study by Engler et al. (*22*) concerning the effect of rigidity on the fate of MSCs; in their study the authors also observed that the effect were abrogated by the addition of blebbistatin, indicating that the rigidity sensing was dependent on actomyosin pathways.

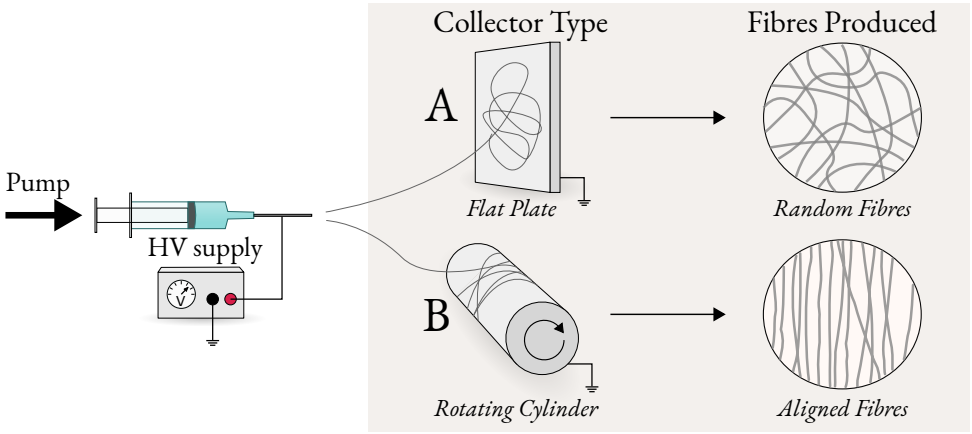

Figure 1.1. Schematic overview of the electrospinning process. A high voltage (HV) source is connected between the nozzle of the syringe and the collector. Using a flat, static collector plate **(A)** leads to random fibres being formed, while using a rotating cylinder **(B)** as the collector yields aligned fibres. The sheet of fibres produced can be cut into suitable shapes for cell culture.

1.4 BIOMIMETIC 3D SCAFFOLDS

As mentioned, several novel types of 3D scaffolds have emerged over the last decades. Some of the more common types are electrospun fibrous scaffolds, decellularized ECM and hydrogels (*37*). These three types of scaffolds will be described below, with extra focus on electrospun fibrous scaffolds, as they are used in the experimental part of this thesis.

Electrospun Fibrous Scaffolds

Electrospinning is a method for producing thin polymer fibres and has been used in various fields—ranging from aerospace technology to textile industry—over the last century (*38*, *39*). Due to its ability to produce ECM-like fibrous structures from biocompatible polymers, electrospinning has more recently gained popularity as a method for producing scaffolds for cell culture and transplantation.

An overview of the electrospinning method is shown in Figure 1.1. The polymer is dissolved in a suitable solvent and placed in a syringe, the nozzle of which is connected to a high voltage source. By placing a grounded collector plate a short distance away from the nozzle of the syringe, an electrostatic force is applied on the dissolved polymer. As a pump slowly pushes the solution out through the nozzle, the electrostatic force on the polymer eventually overcomes the surface tension and a small string of polymer is pulled out towards the collector plate where the fibres start forming a random mesh (see Figure 3.1 in Section 3.1). A sheet of fibres is eventually formed and can be cut into suitable shapes and used for cell culture.

An important advantage of using electrospinning is the ability to fine-tune scaffold prop-

erties by using different materials or changing parameters of the fabrication. Several different polymers have been used to make electrospun fibrous scaffolds for cell culture and have also been FDA-approved for clinical use; most notable perhaps are the biocompatible and biodegradable synthetic polymers polycaprolactone (PCL), poly-L-lactic acid (PLLA) and poly(lactic-co-glycolic acid) (*40*). Many natural materials, such as collagen (*41*), hyaluronic acid (*42*) and silk fibroin (*43*) have also be used for electrospun fibrous scaffolds. Furthermore, blends between synthetic and naturally derived materials have been used to achieve scaffolds with specific mechanical and biochemical properties (*44*, *45*). Furthermore, electrospun fibres with encapsulated drugs or proteins, such as growth factors, have been engineered (*46*, *47*); this enables slow release of biomolecules over extended periods of time, providing additional means of mimicking the biochemical microenvironment.

Several parameters of the electrospinning process can be varied to achieve specific topographical properties of the fibrous scaffold: fibre diameter can be controlled by changing the polymer solution concentration, pump flow rate, applied voltage and distance between nozzle and collector (*48*); uncompressed scaffolds can be achieved by using novel baseplate designs (*49*); and scaffolds with aligned fibres can be achieved by using rotary collectors (*48*, *50*).

Decellularized ECM and Hydrogels

Decellularized scaffolds are produced by removing cells from animal tissue, leaving only the ECM (*51*). The method has been widely used for many types of tissue, such as myocardium, kidney and PNS, but has attracted less interest for the CNS.

Hydrogels are crosslinked networks of hydrophilic polymers, which can be artificial or naturally derived (*52*). The hydrophilic character allows the network to absorb large amounts of water, giving it a gel-like structure, similar to that of the ECM (see Box 1.1). Different polymers can be used for fabricating hydrogels, both natural (e.g. collagen, fibrin and alginate) and synthetic (e.g. polyacrylamide and polyethylene glycol) (*53*). One benefit of hydrogels for regenerative strategies is the possibility of administration via injection, allowing for easy and less invasive implantation. Hydrogels are widely used for research and there are many established protocols for their fabrication, and plenty of commercial products are available (*53*).

1.5 CELL SOURCES

Several different types of cells can be used for CNS *in vitro* modelling or regenerative strategies. Common human cell sources are MSCs, induced pluripotent stem cells and hNPCs, all of which are capable of differentiating into neural phenotypes (*5*, *6*). Stem cells are characterised by their inexhaustible capacity of self-renewing divisions which can produce identical stem cells or mul-

tipotential daughter cells, i.e. cells which can differentiate into several different types of cells (*54*, *55*). A closely related cell type are *progenitor* cells; these differ from stem cells in their limited capacity to divide into new progenitors, and in their more limited differentiation potentiality. Neural progenitor cells, for example, can differentiate into the neuronal and glial cells of the CNS, but are unable to produce the non-neural cell types of the CNS (*54*). Nevertheless, progenitor cells are useful and important tools for *in vitro* studies and is the type used in this thesis.

hNPCs are expanded as neurospheres—free-floating spheroidal clusters of undifferentiated neural stem cells or progenitors (*56*, *57*). The formation of neurospheres is a result of an environment where the cells can grow in suspension cultures in the presence of necessary growth factors. However, as neurospheres grow to sizes around the nutrient diffusion limit, the death rate of the central cells starts rising (*58*); to prevent this, neurospheres are dissociated to single cell suspensions—enzymatically or mechanically—and passaged to new containers. The number of times a cell line has been passaged is often used as an approximate measure of its age. After passaging, single cell suspensions can be frozen, seeded for experiments, or continue being expanded; in experiments where differentiation is desired, the suspensions are plated onto adherent surfaces and cultured in a medium without the aforementioned growth factors. The cells will then begin to differentiate into neurons, astrocytes, and oligodendrocytes (*57*).

1.6 AIMS

The overall goal of this thesis is to study how topography affects the behaviour of hNPCs, and how these effects are altered by inhibition of myosin II via addition of blebbistatin. More specifically we are looking for effects on differentiation rate and fate, viability, as well as nucleus morphology and alignment. These properties will be examined using immunocytochemistry (ICC) with various markers (see Section 2.6). The following hypotheses are the basis of this thesis:

1. Substrate topography has an effect on differentiation capacity, i.e. the capacity for progenitor cells to differentiate into mature glia or neurons; this will be measured by counting cells expressing the progenitor marker SOX2.
2. Substrate topography has an effect on differentiation fate, i.e. whether the fate of a differentiated progenitor cell is *glial* or *neuronal*; this will be measured by quantifying cells expressing glial markers (GFAP) and neuronal markers (βIIIT & MAP2).
3. Substrate topography has an effect on cell nuclei elongation and alignment; this will be measured by analysing the shape and orientation of nuclei stained by DAPI.
4. Inhibition of myosin II disrupts the substrate topography effects on differentiation capacity and fate. This will be examined by culturing cells on 2D and 3D, with and without the addition of blebbistatin.

Chapter 2

Materials and Methods

This section describes the methods used in this thesis, and a short theoretical background is given to certain steps. The thesis is divided into two main projects which will be referred to as *project A* and *project B*; the former is related to hypotheses 1 to 3, while the latter will shed light on hypothesis 4. Cell culture and fixation in project B was performed together with another master student in the lab. An overview of the experimental work is displayed in Figure 2.1.

2.1 PREPARATION OF SUBSTRATES

Electrospun fibrous PCL scaffolds manufactured by Cellevate AB were used in both project A and B. The fibres were electrospun on a thin PLLA backing and were cut into circular shapes and sterilized. In project A, both random and aligned fibrous scaffolds were used, and in project B only random fibrous scaffolds were used. Round glass slides were used as flat substrates in both projects.

All substrates were sterilized in 70 % ethanol. After rinsing with phosphate-buffered saline (PBS), the substrates were coated with poly-L-lysine (PLL) (Sigma-Aldrich; Cat. no P4707) for around 45 min, rinsed with water and then stored in a sterile hood at room temperature (RT) until used in experiments.

2.2 CHARACTERIZATION OF FIBRES

For *project B*, scanning electron microscopy was used to examine the electrospun fibres and measure the fibre diameters. One scaffold was sputtered with 20 nm Au (Cressington Sputter Coater 108 auto, Cressington Scientific Instruments) and was thereafter examined in a scanning electron microscope (SU3500, Hitachi). Fibre diameter measurements were performed using ImageJ (NIH).

2.3 CELL ASSAY AND EXPANSION

The experimental work of this thesis uses hNPCs acquired from the forebrain of a 7 week post-conception human fetus. This line of hNPCs was initially established by Carpenter et al. (*59*) at the Karolinska University Hospital, Stockholm, Sweden, and was provided to us via Prof. A. Björklund (Department of Experimental Medical Science, Lund University, Sweden).

Experimental Work

HNPCs are expanded as neurospheres. When the spheres are large enough, they are dissociated to single cells for continued expansion or for use in experiments. The experimental work is divided into two projects: A and B.

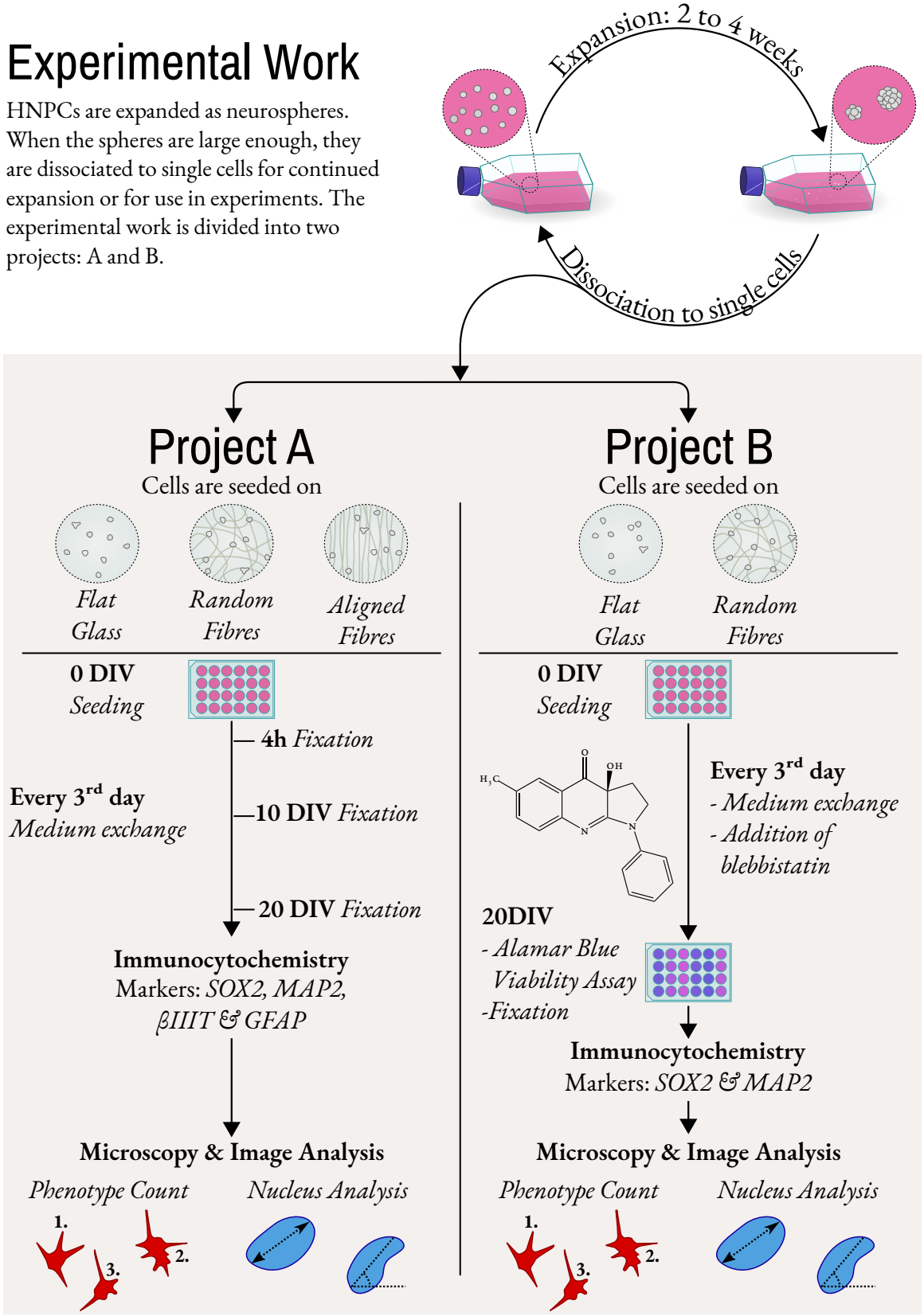

Figure 2.1. Overview of the experimental work of this thesis.

For expansion, hNPCs were cultured as free-floating neurospheres in expansion medium consisting of DMEM/F12 (Gibco; Thermo Fisher Scientific; Cat. no. 21331020) supplemented with 1 % N-2 (Gibco; Thermo Fisher Scientific; Cat. no. 17502048), 2 mM Pen/Strep-L-Glutamine (Gibco; Thermo Fisher Scientific; Cat. no. 10378016), 0.6 % D-(+)-Glucose (VWR Chemicals; Cat. no. 101174Y), 2 $\mu g\,ml^{-1}$ Heparin (Sigma Aldrich; Cat. no. H3149), 20 $ng\,ml^{-1}$ hEGF (Prospec; Cat. no. CYT-217), 20 $ng\,ml^{-1}$ hbFGF (Prospec; Cat. no. CYT-218), and 10 $ng\,ml^{-1}$ hLIF (Prospec; Cat. no. CYT-644); see Box 2.1 for description of the medium composition. Incubation took place in 37 °C with 5 % CO_2 and a relative humidity of 95 %. Dissociation was performed every 2 to 4 weeks using StemPro™ Accutase™ (Gibco; Thermo Fisher Scientific; Cat. no. A1110501). After dissociation, cells were either frozen at −150 °C for later use, seeded into new flasks for further expansion, or used in experiments.

2.4 SEEDING OF CELLS

Cell culture and seeding in *project A* was performed by a previous master student in the lab. Passage 15 to 17 hNPCs were seeded onto glass slides or electrospun fibrous PCL scaffolds (random and aligned). Cells were counted using trypan blue and an automated cell counter (TC20; Bio-RAD). The seeding density was around 90 000 cells/cm^2 for all wells. A total of three different seedings were performed, each on a separate day. In *project B*, passage 14 to 15 hNPCs were seeded onto glass slides or electrospun random fibrous PCL scaffolds. The seeding density was around 90 000 cells/cm^2 for all wells. Here, only one seeding was performed.

Cells in both projects were cultured in differentiation medium consisting of DMEM/F12 (Gibco; Thermo Fisher Scientific; Cat. no. 21331020) supplemented with 1 % FBS (Gibco; Thermo Fisher Scientific; Cat. no. A3840101), 1 % N-2 (Gibco; Thermo Fisher Scientific; Cat. no. 17502048), 2 mM Pen/Strep-L-Glutamine (Gibco; Thermo Fisher Scientific; Cat. no. 10378016), 0.6 % D-(+)-Glucose (VWR Chemicals; Cat. no. 101174Y), and 2 $\mu g\,ml^{-1}$ Heparin (Sigma Aldrich; Cat. no. H3149); see Box 2.1 for a description of the medium composition. Culturing took place in 37 °C with 5 % CO_2 and a relative humidity of 95 %.

In *project A* medium was replaced every second or third day until termination at 4 h, 10 days *in vitro* (DIV) or 20 DIV. In *project B*, cell cultures were divided into three groups: one negative control group cultured in normal medium; one myosin II-inhibited group cultured in medium supplemented with 5 μM blebbistatin dissolved in 0.15 % DMSO; and one vehicular control group cultured in medium supplemented with 0.15 % DMSO. The medium was replaced every third day until termination at 20 DIV. Before each medium exchange, phase contrast microscopy (Olympus; CKX53) was used to capture images of the cells grown on glass slides.

Box 2.1: Culture Media

Three types of cell culture media were used in my experiments: basic medium, expansion medium, and differentiation medium; all of these are based on the media used by Carpenter et al. (*59*). Basic medium was not used for cell culture *per se*, but rather served as the base for the other two types of media. Below is a description of the ingredients of the three types of media. More details on the recipes can be found in Appendix C.

Basic Medium

Ingredient	Description
DMEM/F12	1:1 mixture of Dulbecco's Modified Eagle Medium and Ham's F12 Nutrient Mixture; provides a high concentration of amino acids, vitamins and other nutrients. Used for many different kinds of mammalian cell culture.
Pen/Strep	Mixture of penicillin and streptomycin, to prevent bacterial infections
Glucose	Supplemental glucose.
N-2 Supplement	A supplement developed specifically for neural cell cultures.
Heparin	Needed for hbFGF stimulation (*60*).

Expansion Medium

Ingredient	Description
Basic medium	Base of the medium.
hEGF	Human epidermal growth factor. Appears to increase proliferation in the cell line but does not seem necessary for maintenance and survival (*59*)
hbFGF	Human basic fibroblast growth factor. Has been shown to increase rate of proliferation and promote neuronal differentiation in the cell line after seeding (*59*).
hLIF	Human leukemia inhibitory factor. Similar effects to those of hbFGF have been observed (*59*).

Differentiation Medium

Ingredient	Description
Basic medium	Base of the medium
FBS	Fetal bovine serum. Extracted from the blood of a bovine fetus. Contains an undefined mixture of growth factors, hormones, proteins, vitamins and more (*61*).

2.5 ALAMAR BLUE VIABILITY ASSAY

The Alamar Blue viability assay is a commonly used method for quantifying cell culture viability. The active component of Alamar Blue is resazurin. Alamar Blue comes in an oxidized, non-fluorescent state, but when incubated with live cells it acts as an electron acceptor in the electron transport chain and is subsequently reduced to a fluorescent state. The concentration of the fluorescent form is thus proportional to the number of live cells in the sample. By measuring the fluoroscence (or absorbance) of Alamar Blue after incubation with cells, and comparing it to a control, the viability of a cell culture can be quantified (*62*).

An Alamar Blue viability assay was performed in *project B* to measure the viability of cells after 20 DIV. Cells were incubated for around 3 hours in differentiation medium supplemented with 10 % Alamar Blue (Invitrogen; Thermo Fisher Scientific; Cat. no. DAL1025). Thereafter media from all wells were transferred to a 96-well plate, and fluorescence was measured with an emission wavelength of 590 nm and an excitation wavelength of 485 nm.

2.6 FIXATION AND IMMUNOCYTOCHEMISTRY

ICC is a method which uses antibodies to label proteins and molecules in cells and tissue (*63*). This method can be categorised into two main types: *direct* and *indirect*. In direct ICC, antibodies conjugated with fluorophores bind to a specific antigen. Using fluorescence microscopy, the location of these antigens in a biological sample can be determined. In indirect ICC, two different types of antibodies are used: primary, which bind to the antigen, and secondary, which bind to the primary antibodies and are conjugated with fluorophores (*63*). For the experiments in this thesis, indirect ICC was used to identify various proteins associated with different fates of hNPCs; the choice of indirect ICC was based on cost and flexibility. To make full use of the material, double staining was always employed.

Procedure

All cells were fixed in 4 % paraformaldehyde (PFA) in phosphate-buffered saline (PBS) at room temperature and thereafter rinsed three times with PBS and stored in PBS at 4 °C until used in ICC. Incubation with primary antibodies was done at 4 °C for at least 12 h in blocking buffer consisting of 1 % bovine serum albumin (BSA) and 0.25 % Triton-X in PBS. Following the incubation, the samples were washed three times in PBS. Incubation with secondary antibodies was performed in the dark at room temperature for 1 h in blocking solution. Thereafter samples were washed again three times before they were mounted on glass slides using Vectashield® Antifade Mounting Medium with DAPI (Vector Laboratories; Cat. no. H-1200).

Choice of Neural Markers

SOX2 as a marker for progenitor cells Sex determining region Y-box 2 (SOX2) is a transcription factor discovered by Gubbay et al. (*64*) and Dailey et al. (*65*), and is involved in the maintenance of neural stem cells and precursors. SOX2 is expressed in the nuclei of neural progenitor cells until their final cell cycle before differentiation, and functions to inhibit neuronal differentiation (*66*). SOX2 will thus serve as a marker for undifferentiated hNPCs in this project.

GFAP as a marker for glial differentiation Glial fibrillary acidic protein (GFAP) is the main major component of glial filaments, a class of intermediate filament predominantly found in mature astrocytes (*67*). However, it has also been shown in mouse, that GFAP is expressed in progenitors which through division give rise to immature neurons (*68*).

βIIIT and MAP2 as markers for neuronal differentiation Class III β-tubulin (βIIIT) is one of several isoforms of tubulin, a globular protein which is the principal component of microtubules. Of all isoforms, βIIIT is unique in the sense that it is believed to be almost exclusively expressed in neurons (*69*). However, some studies have show that βIIIT is not *always* neuron-specific: expression of βIIIT has also been shown to be expressed in fetal astrocytes (*70*), as well as in different kinds of brain tumours (*71*).

Microtubule-associated protein 2 MAP2 belongs to a family of proteins which bind to and stabilize microtubule (*72*). Several proteins in this family, including MAP2, are believed to be neuron-specific. MAP2 consists of three polypeptides MAP2a, MAP2b, and MAP2c, of which the latter is only present in the juvenile brain (*73*). While MAP2a and MAP2b indeed are neuron-specific, MAP2c has also been shown to be expressed in GFAP+ precursors (*74*), a commonly overlooked problem when attempting to identify neurons (*75*).

Antibodies Used

Table 2.1 and Table 2.2 on the next page show the primary and secondary antibodies used for this thesis. All antibodies were tested by omitting each primary antibody and incubating with secondary antibodies; this was done to ensure specificity and to find suitable dilutions.

2.7 MICROSCOPY AND IMAGE ANALYSIS

Microscopy was performed using a ZEISS Axio Imager 2 microscope. For each well, 3 to 4 areas, preferably one in each of the four corners of the sample, and with an adequate number of cell nuclei, were selected in a pseudo-random fashion. By viewing only the DAPI-channel when selecting the areas, bias for any specific morphology or expression is reduced. One photograph was

taken for each channel and area and saved in a lossless .tif format.

Nuclei and SOX2+ cells were counted using a semi-automatic approach: a python script using functions from the sci-kit image package (*76*) was written to segment the DAPI- or SOX2-channel of each image; each segmented image was thereafter checked manually to remove possible double counts or missed counts. GFAP+, MAP2+ and βIIIT+ cells were counted manually. A Python script using functions from the sci-kit image (*76*), OpenCV (*77*) and NumPy (*78*) libraries was written and used for the nucleus analysis.

2.8 STATISTICAL ANALYSIS

All statistical work was done in Python using the scipy (*79*) and statsmodel (*80*) libraries, and all graphs were constructed using the Matplotlib library (*81*). Differences between groups are measured by a one-sided analysis of variance (ANOVA) combined with Tukey's HSD, with $p \leq 0.05$ considered significant. Statistics are presented as mean $\pm$ standard error of the mean (SEM) unless stated otherwise. Different biological replicates are defined as separate seedings on different days, while technical samples are from the same seeding, but different wells. Three different significance levels are used for presentation in the graphs: $p \leq 0.05$ (*), $p \leq 0.01$ (**), and $p \leq 0.001$ (***). In project A, $n = 3$ biological replicates were used for most measurements, while in project B $n = 1$ biological replicate was used; statistical analysis using ANOVA was thus not used for project B.

Table 2.1. List of Primary Antibodies

Antigen	Host	Target Cell	Dilution	Source	Cat. No.
βIIIT	Mouse	Early Neurons	1:2000	Sigma-Aldrich	T8660
GFAP	Rabbit	Glial Cells	1:2000	Dako	Z0334
SOX2	Mouse	Progenitor Cells	1:1000	Santa Cruz Biotechnology	sc365964
MAP2	Chicken	Neurons	1:2000	Abcam	ab5392

Table 2.2. List of Secondary Antibodies

Host	Target	Fluorochrome	Dilution	Source	Cat. No.
Donkey	Mouse	Alexa Fluor® 488	1:400	Invitrogen Thermo Fisher Scientific	A21202
Goat	Rabbit	Alexa Fluor® 594	1:400	Invitrogen Thermo Fisher Scientific	A11037
Rabbit	Chicken	Texas Red®	1:200	Abcam	ab6751

Chapter 3

Results

3.1 CHARACTERIZATION OF ELECTROSPUN FIBROUS SCAFFOLDS

A top-view scanning electron microscopy image of the random electrospun fibres is displayed in Figure 3.1 (left). Ten different images from different regions of the scaffold were used for measuring fibre diameters. The average diameter was 769 nm ($n = 1431$), with a median of 635 nm, highlighting the skewed distribution visible in the histogram in Figure 3.1 (right). Characterization of the aligned fibres, which were used in project A, has been done previously (*50*).

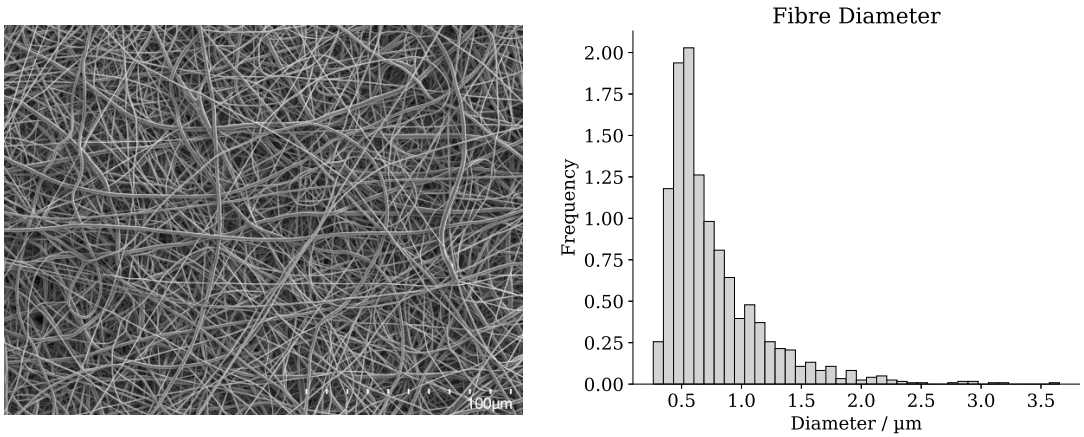

Figure 3.1. Characterization of random fibres. A scanning electron microscopy top-view image of random electrospun fibres is shown in the left image. To the right is a histogram of measured fibre diameters ($n = 1431$) measured in 10 different images of the same scaffold.

3.2 TOPOGRAPHY EFFECT ON DIFFERENTIATION

General Observations

Cell count and density had generally increased from 0 DIV to the later time points. However, for a majority of the random fibre samples, and a few of the aligned, cell count was very low for the later time points. Furthermore, due to the long time between fixation and staining, some of the samples appeared to have dried. Due to this, cell counting was not possible for certain samples.

Overall Differentiation Capacity

The fraction of SOX2+ cells was quantified to examine the differentiation capacity of hNPCs cultured on different substrates. Figure 3.2 shows the percentage of SOX2+ cells over time for cultures on glass slides, random fibrous scaffolds or aligned fibrous scaffolds. As can be seen, the number of SOX2+ cells was high for all groups at all timepoints, indicating low differentiation. Unexpectedly, the expression increased in all groups from 0 DIV to 10 DIV, albeit not significantly. The majority of SOX2- cells at 0 DIV were also MAP2-, likely indicating that these cells are neither progenitor cells or their neuronal progeny. From 10 DIV to 20 DIV there was a slight, but insignificant decrease in SOX2+ cells in the group grown on glass slides, possibly suggesting differentiation into mature cell types. To conclude, phenotypic differentiation was slow for all substrates and no significant differences could be found.

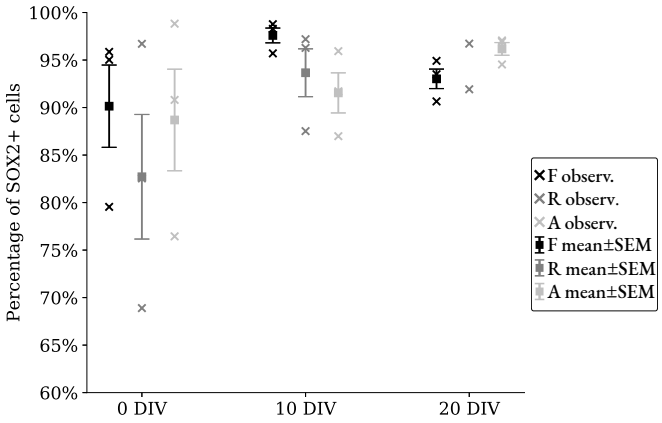

Figure 3.2. Quantification of SOX2+ cells over time. F = cells cultured on flat glass slides; R = cells on random fibrous scaffolds; and A = cells on aligned fibrous scaffolds. The mean of each seeding and group is displayed as a data point; the mean±SEM for these point is also shown. $n = 3$ biological replicates for each group except for random 20 DIV where $n = 2$ due to poor samples. Each biological replicate consists of 2 to 3 technical replicates. No significant differences were found between groups or timepoints.

Phenotypic Differentiation Fate

To examine the effect of topography on glial differentiation, the fraction of GFAP+ cells was quantified. Figure 3.4 shows the percentage of GFAP+ cells over time. As evidenced by the data, GFAP was present in the majority of cells at all timepoints with a consistent percentage of GFAP+ cells of around 60 % for all groups and timepoints. No significant differences were present between any groups or timepoints. The morphologies of GFAP+ cells are changing over time (*cf.* Figure 3.3 above with Figure B.1 & B.2 in Appendix B), with dense networks present in the later

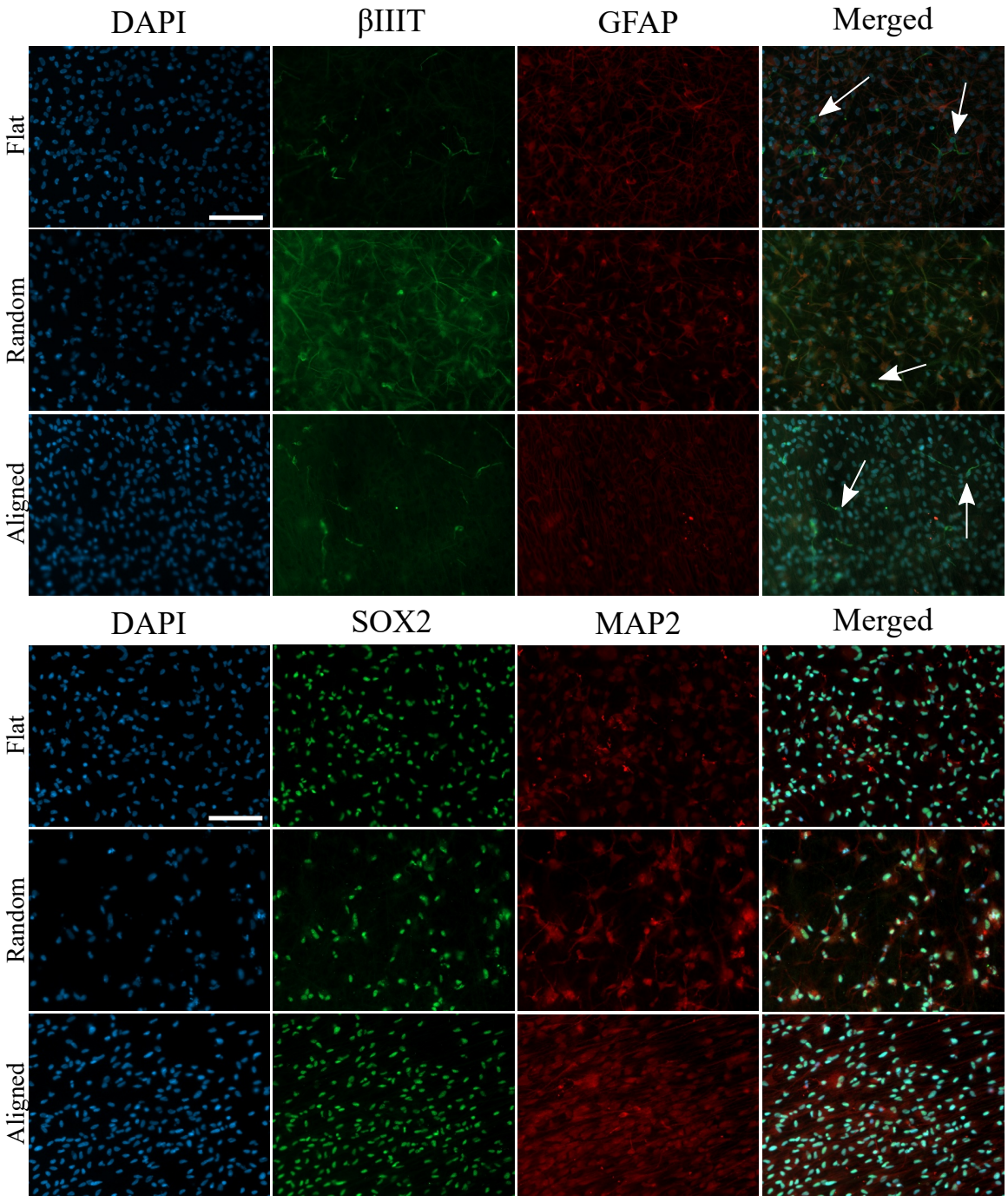

Figure 3.3. Fluorescence microscopy images at 20 DIV. The arrows show examples of neurons, characterized by their stronger βIIIT expression, neuronal morphology and absence of GFAP. Neurons stained by MAP2 are more difficult to distinguish, and more clear examples are shown in Figure 3.5. Notice the alignment of cells cultured on aligned fibres. Scale bars are 100 μm.

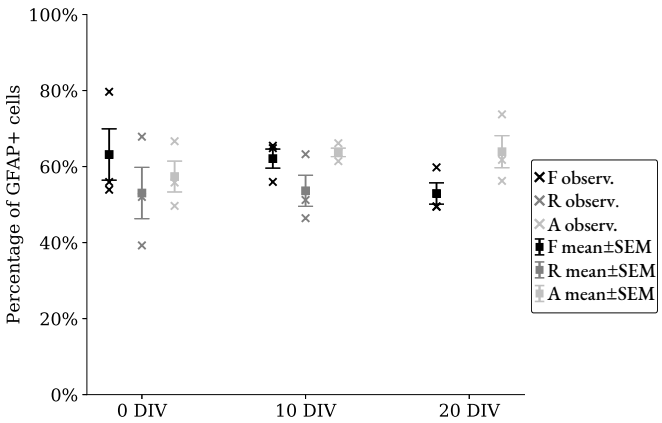

Figure 3.4. Quantification of GFAP+ cells over time. F = cells cultured on flat glass slides; R = cells on random fibrous scaffolds; and A = cells on aligned fibrous scaffolds. The mean of each seeding and group is displayed as a data point; the mean±SEM for these point is also shown. $n = 3$ biological replicates for each group except for random 20 DIV which is omitted due to poor samples. Each biological replicate consists of 2 to 3 technical replicates. No significant differences were found between groups or timepoints.

timepoints. The GFAP+ cells generally have large cell bodies, with thicker outgrowths than those of neurons; on the flat glass substrate GFAP+ cells have very flat *"fried egg"*-like appearances.

Interestingly, there must be an overlap in expression of GFAP and SOX2 at all timepoints as they are both expressed by a majority of cells. This raises the question whether GFAP expression alone truly is an indicator of glial differentiation.

To identify neuronal differentiation, the fractions of βIIIT+ cells and MAP2+ cells, respectively, were quantified. However, these protein expressions were not straightforward to quantify. βIIIT—commonly used as a marker for early neurons—was present around most cells at all time points, for most of the part by cells without neuronal morphology and with co-expression of GFAP. However, at 10 DIV, and even more so at 20 DIV, a stronger expression of βIIIT could be observed for certain GFAP- cells; the shape of this expression was also more neuronal-like, i.e. tighter around the cell nuclei and with thinner and more defined outgrowths (Figure 3.5). These cells were a surprisingly small minority at 20 DIV, however, but based on morphology and GFAP co-expression, none of the other weaker βIIIT+ cells could be confidently identified as early neurons. Figure 3.6 shows the percentage of cells with strong, neuronal-like βIIIT expression. There are no significant differences between the substrates. Nevertheless, for cells grown on flat glass slides, the number of positive cells increased steadily over time, with a significant difference ($p \leq 0.01$) from 0 DIV to 10 DIV. The expression also increased from 0 DIV to 10 DIV in the two fibrous scaffold groups, albeit not significantly. At 20 DIV, the βIIIT+ cell count on aligned fibres is very spread, with one seeding exhibiting the highest count of all groups, while that of the others is much lower.

MAP2—commonly used as a marker for more mature neurons—showed a pattern of expression to that of βIIIT, with a weaker non-neuronal-like expression present for most cells, and a minority of cells with stronger, more neuronal-like expression at later timepoints; this minority of cells also seemed to have a non-existent or much lower expression of SOX2, indicating differentiation. The counting of these neuronal-like MAP2+ cells shows a pattern very similar to that of the βIIIT+ cells (see Figure 3.6), but with an overall slightly lower percentage of positive cells. There were no significant differences between different substrates, but significant differences were present between different timepoints: for cells cultured on flat glass slides there was a significant difference in positive cells from 0 DIV to 10 DIV ($p \leq 0.05$) and from 0 DIV to 20 DIV ($p \leq 0.01$); for cells cultured in aligned fibres there was a significant differences from 0 DIV to 10 DIV ($p \leq 0.05$).

While the overall percentage of cells identified as neurons is small, there were some areas in certain samples where the percentage was much higher, and networks of neurons could be seen. Examples of such areas are shown in Figure 3.5. The neuronal-like MAP2+ and βIIIT+ cells in the flat group were generally located in a layer on top of the rest of the cells, as noticed by adjusting the focal length of the microscope. For the fibrous scaffold samples on the other hand, the neuronal-like cells were more spread in the z-axis.

3.3 TOPOGRAPHY EFFECT ON NUCLEUS MORPHOLOGY AND ALIGNMENT

To examine the morphology and alignment of cell nuclei, the DAPI channel of each image (from the MAP2 and SOX2 staining) was converted to a binary image using an Otsu threshold. Watershed-based segmentation was used on the binary image to detect single nuclei. For each nucleus, an ellipse with the same second central moments was identified; the area, orientation and elongation (defined as the major axis divided by the minor axis) were calculated for each ellipse. A lower limit for area was set to remove regions too small to be nuclei. Nuclei were analyzed in terms of elongation and alignment.

Nucleus Elongation

The results of the elongation measurements are displayed in Figure 3.7. The data shows that the cells cultured on aligned fibrous scaffolds or flat 2D surfaces exhibited the most elongated nuclei, with significant differences compared with the random fibre group on 10 DIV. While there are no significant differences between nuclei on aligned fibres and flat 2D surfaces, the former appear to be more elongated at all timepoints. Elongation increases significantly from 0 DIV to 10 DIV in the aligned and flat groups, but does not seem to have increased further at 20 DIV.

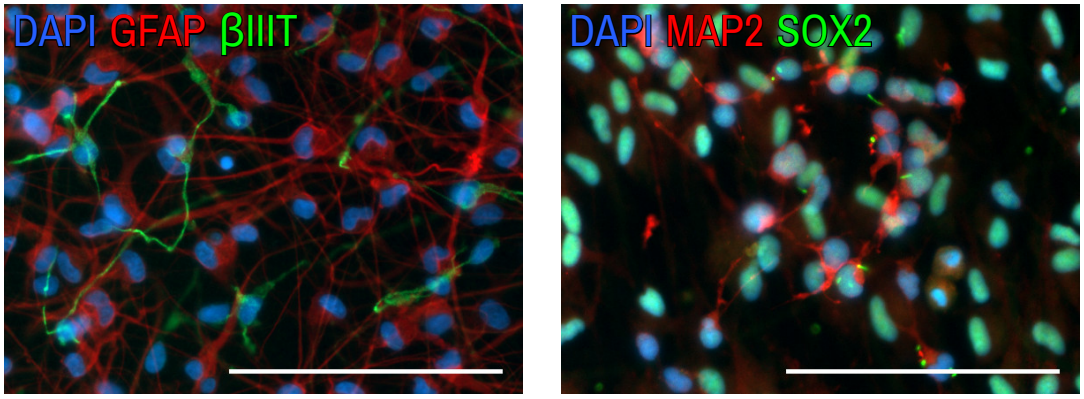

Figure 3.5. Fluorescence microscopy at 20 DIV showing clear neuronal differentiation. The cells in the image on the left are cultured on flat glass slides and double stained with GFAP (red) and βIIIT (green), and counterstained with DAPI (blue). The βIIIT+ cells are GFAP- and show neuronal morphologies; they can be seen lying on top of a network of GFAP+ cells. The cells in the right image are cultured on aligned fibrous scaffold and double stained with MAP2 (red) and SOX2 (green), and counterstained with DAPI (blue). The MAP2+ cells have neuronal morphologies, and show low or non-existent expression of SOX2. Scale bars are 100 μm

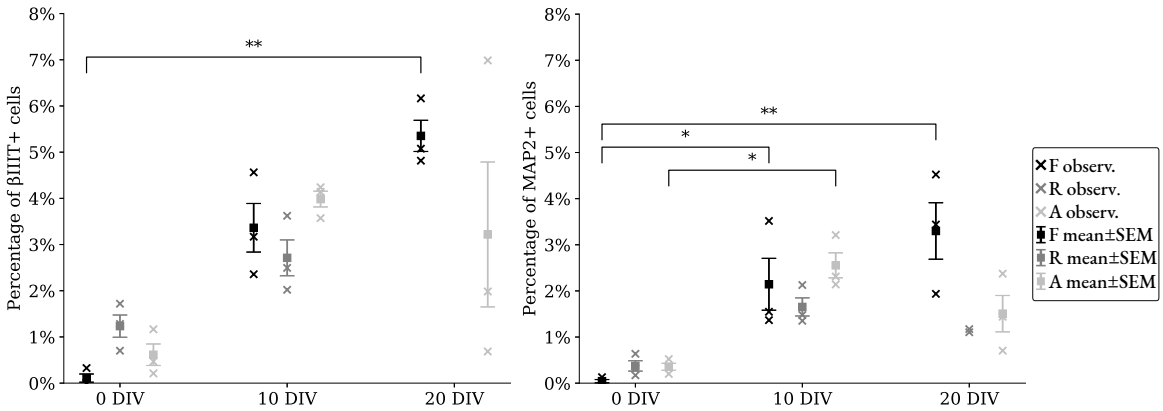

Figure 3.6. Quantification of βIIIT+ and MAP2+ cells over time. F = cells cultured on flat glass slides; R = cells on random fibrous scaffolds; and A = cells on aligned fibrous scaffolds. The mean of each seeding and group is displayed as a data point; the mean±SEM for these point is also shown. $n = 3$ biological replicates for each group except for random 20 DIV where $n = 2$ in for MAP2 and, and omitted completely for βIIIT due to poor samples. Each biological replicate consists of 2 to 3 technical replicates. Significance levels: (*) $p \leq 0.05$; (**) $p \leq 0.01$; and (***) $p \leq 0.001$.

Effect on Nucleus Orientation and Alignment

To measure and compare nuclear alignment, the standard deviation σ of all nuclear orientations in a sample is a useful parameter, with a smaller σ indicating better alignment and a larger σ indicating a more uniform distribution. In a paper by Davidson et al. (*82*), the authors showed that σ follows Gaussian law and can be used by Gaussian statistical tools such as ANOVA.

The method for obtaining σ is inspired by the methods used by Yang et al. (*83*). First, nuclear orientations from each sample are calculated in relation to a 0° reference angle (image x-axis) and subsequently shifted to the interval $[-90°, 90°]$. Only nuclei with an elongation ratio over 1.5 were used in order to limit the statistics to nuclei with a clear orientation. For each sample σ is then calculated. The reference angle is thereafter shifted 1° and σ is recalculated; this is repeated until the reference angle has reached 179°. The reference angle which yields the lowest σ, i.e. best alignment, was noted and this σ was saved for statistical comparison. For sample with a completely uniform distribution of orientations $\sigma = 52°$, and for a sample where all nuclei have exactly the same orientation $\sigma = 0°$

The orientations for all nuclei at 20 DIV, normalized to the reference angle yielding the lowest σ, are presented in the histogram in Figure 3.8 (left). The σ for each group and timepoint and presented in Figure 3.8 (right). The histogram shows a clear difference in alignment between cells grown on aligned fibrous scaffolds compared to the other substrates. The results of the σ comparison support this notion, with significant differences in alignment present at all timepoints.

3.4 EFFECTS OF MYOSIN II INHIBITION

Seeding and Culture of Cells in Project B

Directly after seeding, cell density and adhesion both appeared normal in all wells. After 4 h, however, phase contrast microscopy revealed floating cells, generally low cell density as well as large areas without any cells. Over the next several days, the cell density gradually increased to more normal levels. Phase contrast microscopy is not possible for cells on fibrous scaffolds and thus nothing could be told about the 3D groups until fixation and ICC.

After the addition of blebbistatin at 1 DIV cell morphologies started changing compared to the DMSO vehicular control and pure medium negative control; cells cultured with blebbistatin exhibited thinner outgrowths and less pancake-like appearance. Figure 3.9 shows a comparison of cells in blebbistatin and negative control at 7 DIV.

During the last few days before fixation, both negative and DMSO vehicular control groups showed signs of apoptosis, with floating cells and empty circular areas starting to form; the same could not be observed for the blebbistatin groups. Furthermore, the cell density appeared higher in both control groups compared to that of the blebbistatin treated group (see Figure 3.10).

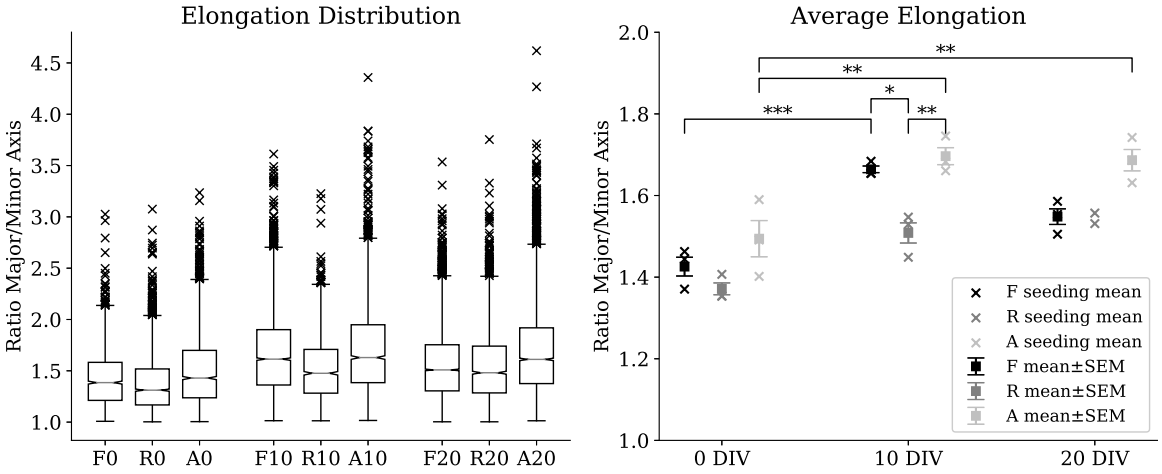

Figure 3.7. Results of the nucleus elongation analysis. Box plots (with outliers) of all elongation measurements, pooled from all seedings, are displayed in the left image; between 1546 to 8055 nuclei were analyzed per group. In the graph on the right, the mean of the each seeding and group is displayed as a data point; the mean±SEM for these point is also shown. $n = 3$ biological replicates for each group except for random 20 DIV where $n = 2$. Each biological replicate consists of 2 to 3 technical replicates. Significance levels: (*) $p \leq 0.05$; (**) $p \leq 0.01$; and (***) $p \leq 0.001$.

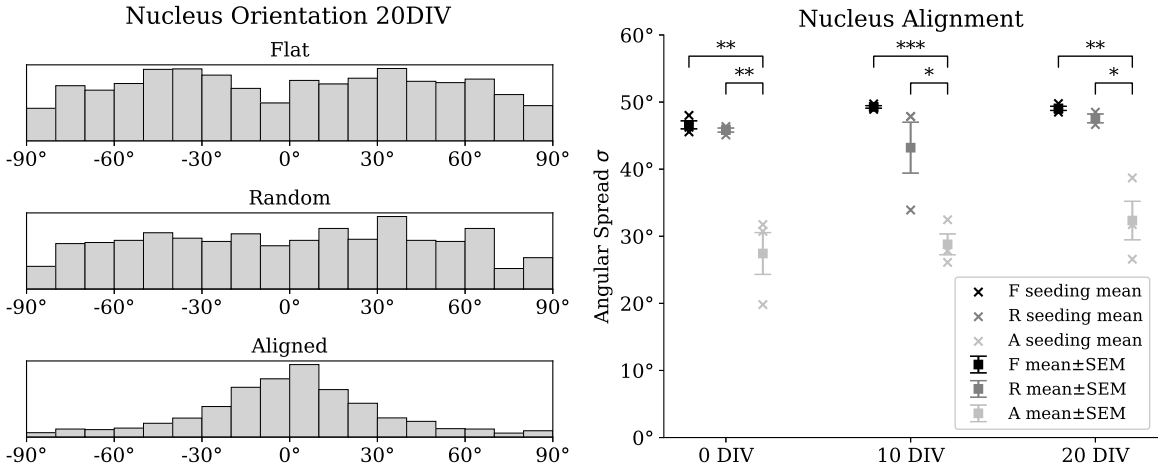

Figure 3.8. Results of the nucleus alignment analysis. Nucleus orientations are normalized to the reference angle which yields the highest alignment of each sample. To the left, the orientations at 20 DIV from all seedings are pooled together and shown in histograms; 792 to 2287 nuclei were analyzed for each group. To the right, the mean of the angular spread σ (described in the text) for each seeding and group is displayed as a data point; the mean±SEM for these point is also shown. $n = 3$ biological replicates for each group except for random 20 DIV where $n = 2$. Each biological replicate consists of 2 to 3 technical replicates. Significance levels: (*) $p \leq 0.05$; (**) $p \leq 0.01$; and (***) $p \leq 0.001$.

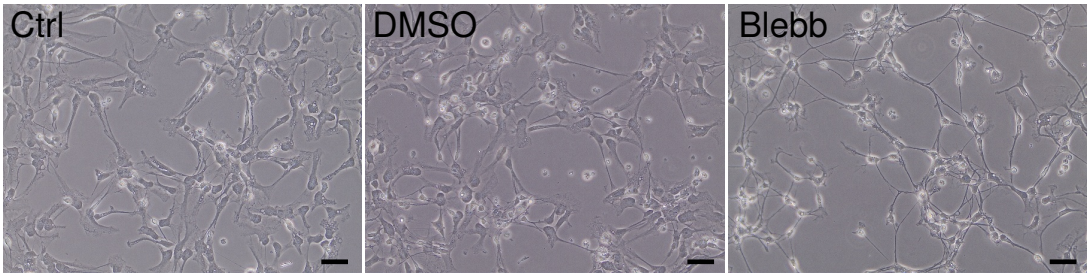

Figure 3.9. Phase contract microscopy images at 7 DIV. Note the obvious differences in morphology between the two control groups, and the blebbistatin-treated group. Scale bars are 50 µm.

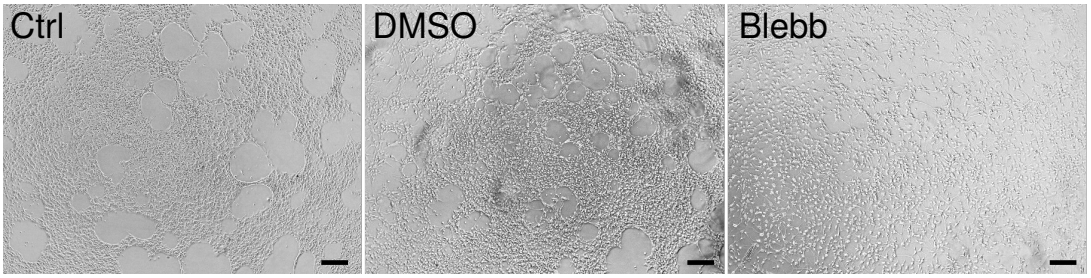

Figure 3.10. Phase contrast microscopy images at 19 DIV. During the last few days *in vitro*, circular holes devoid of cells started forming in the negative and vehicular control groups; these holes were not present in the groups treated with blebbistatin. Cell density also appears much higher in the two control groups. Scale bars are 200 µm.

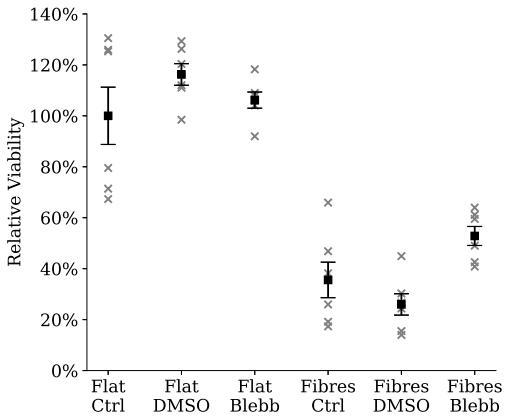

Figure 3.11. Results of the Alamar blue viability assay at 20 DIV. $n = 6$ wells were analyzed per group. Each data point represents the viability of a single well, normalized to the average of the control group, and is presented with mean±SEM for each group.

The results of the Alamar blue viability assay performed at 20 DIV are displayed in Figure 3.11. There are large differences in viability between cells grown on glass slides and cells grown on electrospun fibrous scaffolds. However, there are no clear differences in viability between groups treated with different chemicals.

Effect of Blebbistatin on Differentiation Fate and Capacity

In line with the results of the viability assay, immunostaining revealed traces of extensive apoptosis for all groups on fibrous scaffolds, with insufficient material for phenotypic analysis. Thus, nothing can be said about hypothesis 4. However, the effects of myosin II inhibition on hNPCs cultured on glass slides was still examined.

Quantification of SOX2+ cells and MAP2+ cells is shown in Figure 3.13 and indicates a majority of progenitor cells for all groups. The DMSO and blebbistatin groups appear to have slightly larger percentages of differentiated cells. However, the blebbistatin group was very spread, with two wells with less differentiation and one well with surprisingly high differentiation. The same differences are mirrored in the MAP2 quantification: here only a few percent of cells had differentiated into neurons in the control group, while an average of around 8 % had differentiated into neurons in the DMSO and blebbistatin groups. The neuronal differentiation capacity was large in the blebbistatin group, with one well exhibiting up to 14 % differentiated neurons.

In the DMSO and negative control groups, cells were not evenly spread on the substrate but appeared to often stick together forming local dense regions. Neuronal differentiation appeared to be more present in these denser regions. In the blebbistatin group, cells were generally more homogeneously spread and neuronal differentiation did not seem to be as affected by cell density.

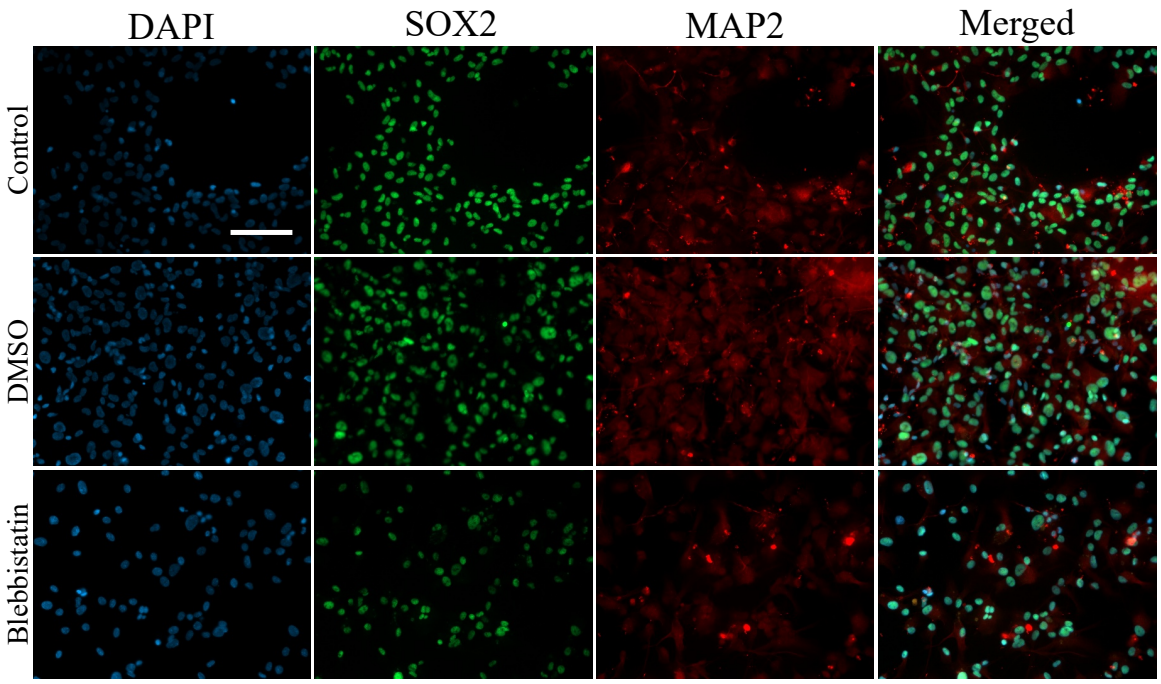

Figure 3.12. Fluorescence microscopy images at 20 DIV. The circular holes previously mentioned can be clearly seen in the negative control group. The higher cell density of both control groups is also visible.

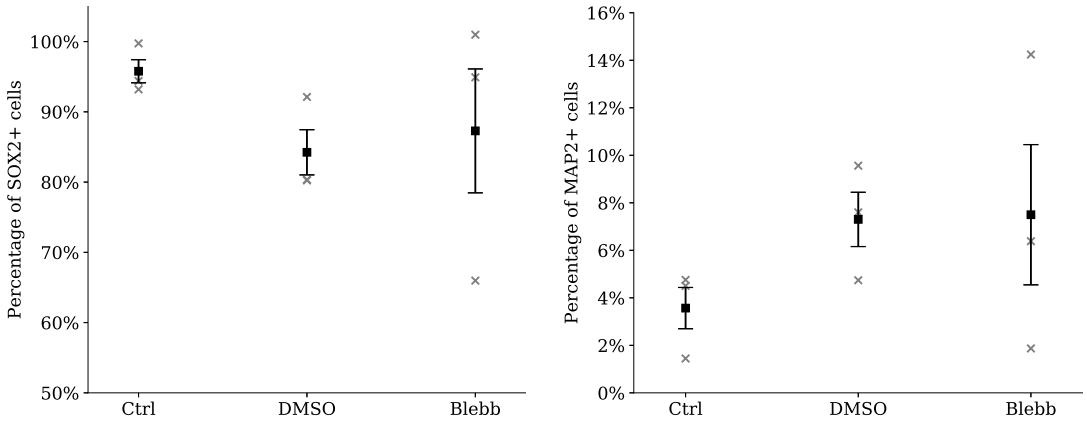

Figure 3.13. Quantification of SOX2+ cells (left) and MAP2+ cells (right) at 20 DIV for hNPCs seeded on flat glass slides. The mean of each well and group is displayed as a data point; the mean±SEM for these point is also shown. $n = 3$ *technical* replicates for each group.

Nucleus Elongation Analysis

Following the procedure described in Section 3.3. The nuclei of the different groups were analyzed in terms of elongation. The results are displayed in Figure 3.14 and indicate that myosin II inhibition with blebbistatin has an effect on nucleus morphology. Cells treated with blebbistatin exhibit rounder nuclei than those of the vehicular control or negative control groups.

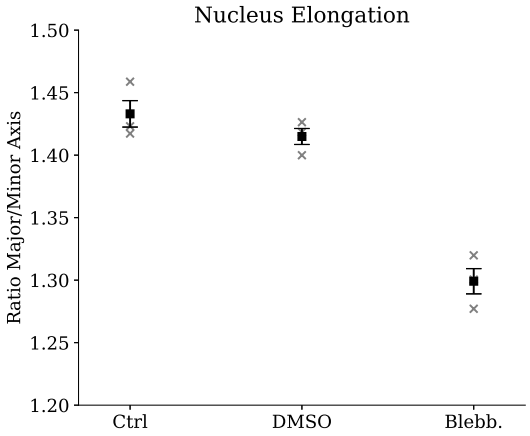

Figure 3.14. Results of the nucleus elongation analysis. Cells treated with blebbistatin consistently exhibit lower nucleus elongation.

Chapter 4

Discussion

Control over phenotypic differentiation is important in both *in vitro* disease modelling and cell-based regenerative therapies. Here we investigated how the topography of electrospun fibrous scaffolds affects differentiation of hNPCs; we examined differentiation in terms of overall capacity as well as phenotypic fate. Furthermore, we analyzed how topography affects cell nucleus morphology and polarization. Finally, to elucidate pathways responsible for potential effects, we inhibited myosin II via the addition of blebbistatin to see if any topographical effects remain.

Our results show no significant differences in differentiation capacity or fate between groups grown on glass slides, random fibrous scaffolds or aligned fibrous scaffolds. Nevertheless, we found significant differences in nucleus elongation and alignment between the groups.

As our cell cultures on fibrous scaffold with addition of blebbistatin suffered from low viability, the effects of myosin II inhibition remain unclear in these cultures. However, our results suggest that the addition of blebbistatin to cultures on glass slides might affect cell differentiation and nucleus morphology. Below, I interpret and discuss the results in more detail.

4.1 EFFECTS OF SUBSTRATE TOPOGRAPHY ON CELL SURVIVAL

After using immunostaining in project B, we discovered that cell count at 10 DIV and 20 DIV was generally lower for the cultures on fibrous scaffolds—especially for those on random fibres, where some wells were almost completely devoid of cells. In project B, the Alamar blue viability assay showed low viability (Figure 3.11) for groups on fibrous scaffolds compared to those on glass slides. After immunostaining we saw traces of cells, covering the whole sample, on the fibrous scaffolds, but only few cells still present. Lower cell count and lower viability as measured by the Alamar blue assay does not mean poor survival *per se*, as a lower cell density might be more optimal, and high viability measurements can be due to stressed cells (communication with Ulrica Englund-Johansson). However, since the presence of cells was insufficiently large to permit quantitative analysis, the survival cannot be considered optimal. The reasons for the lower survival of hNPCs are unclear and should be investigated further.

4.2 EFFECTS OF SUBSTRATE TOPOGRAPHY ON DIFFERENTIATION

We show slow differentiation of hNPCs on all substrates, with a large majority of cells expressing SOX2 even after 20 DIV. In the original study of the cell line, the authors showed almost

complete differentiation after 7 DIV, with only 5 % of cells being identified as progenitors at this timepoint (*59*). In contrast to previous results (*50*), we also demonstrate that the choice of substrate has no significant effect on neuronal differentiation fate of hNPCs. The question arises whether substrate truly has no effect, or if there might be differences between different substrates but the overall differentiation is too slow for any effects to be visible after 20 DIV.

Quantification of βIIIT+ cells and MAP2+ cells

MAP2 and βIIIT expressions were difficult to quantify. βIIIT was expressed in nearly all GFAP+ cells, and similarly MAP2 was expressed in nearly all SOX2+ cells; furthermore, these cells did not exhibit typical neuronal morphologies. However, there were cells with clear neuronal morphology and neural marker expression and these were the basis for our inclusion criteria for the neuron quantification. The number of βIIIT+ cells was generally higher than that of MAP2+ cells which was expected as MAP2 is generally used as a marker for more mature neurons.

Quantification of βIIIT+ cells and MAP2+ cells was made difficult by the fact that neurons often lay at a different focal depth compared to other cells; this was especially true for cells grown on fibres, as their topography permits larger cell spread in the z-axis, a phenomenon which has been observed and quantified in previous studies in our lab (*50*). As a result, it was difficult to capture images where all cells could be seen sharply enough to be quantified, and more neurons might have been missed in the fibrous scaffold groups. To improve quantification, and make it more consistent between the different substrates, other analytical methods could be employed. One option is using confocal microscopy with z-stack imaging. This could be combined with flow cytometry and/or Western blotting, to get different measurements of protein expression in the samples.

Quantification of GFAP+ Cells

The number of GFAP+ cells was relatively constant throughout the culture and there were almost no differences between groups. It is unclear whether these GFAP+ cells truly are mature astrocytes. Research has shown that GFAP is expressed in progenitor cells which can give rise to neuronal progeny (*68*). As mentioned there must be a large overlap in GFAP and SOX2 expression, and this could be explained by the fact that GFAP+ cells not necessarily are astrocytes, but a type of glial progenitor cell.

Potential Reasons for Slow Differentiation

The cell line used has the capacity of neuronal differentiation, as evidenced by the clear neuronal morphologies and expression of neuronal markers observed in some samples. Nevertheless, dif-

ferentiation is slow and the reason for this is unclear as the methods are close to identical to those of previous studies in our lab (*50*) which have shown faster differentiation. There are some differences however: the hNPCs in the present study were from a relatively late passage 15 to 17, and differentiation of the cell line has been shown to vary with different passage numbers (*59*). This could be explained by the drift of cell lines over time if they are heterogeneous and non-immortalized (communication with Ulrica Englund-Johansson).

In this thesis I have focused on topographical effects on hNPC behaviour. It is possible, however, that certain biochemical parameters are lacking which may promote differentiation of our cell line. For example, our substrates are coated with PLL to improve adhesion, but additional coating with ECM proteins, such as laminins or fibronectins, or with artificial peptide sequences such as Arg-Gly-Asp could furthermore promote cell survival and differentiation. Unpublished work from our lab suggests that coating substrates with various laminins may have an effect on both hNPC survival and overall differentiation capacity.

Apart from ECM proteins, certain growth factors might be in low concentration in our medium. Differentiation media are commonly supplemented with 10 % FBS in order to attain a suitable concentration of growth factors needed for differentiation. The differentiation medium used in this thesis is based on the medium originally used by Carpenter et al. (*59*) for the same cell line, and contains only 1 % FBS. While this lower concentration has worked well in many studies, it might not be sufficient under all conditions. Furthermore, the biochemical composition of FBS may vary substantially between manufacturers and different batches (*84*). For more consistency between studies, a better approach would be to use a chemically defined medium. Unpublished work from our group has shown that hNPCs cultured in chemically defined BrainPhys™ medium exhibited more neuronal differentiation compared to those cultured in the same differentiation medium used in this thesis.

Another potential issue with our medium may be the high concentration of glucose. The concentration of glucose in DMEM/F12 is 17.5 mM, which is already 2 to 5 times higher than what has been observed in *hyperglycemic* patients (*85*). Addition of supplemental glucose according to our medium recipe yields a total glucose concentration of around 40 mM, many times higher than that in a normal adult brain. While we are using hNPCs from fetal forebrain, and the developing brain does require higher glycemic levels than the adult brain (*86*), it would be surprising if *such* a high concentration really is needed. Furthermore, high glucose levels has been shown to inhibit neural stem cell differentiation (*87*) and proliferation (*88*); and interestingly, both of these studies defined a high glucose concentration as 25 mM, i.e. only around 60 % of that of our medium. As previously mentioned, hNPCs cultured in BrainPhys™ medium—which has a glucose concentration around 2.5 mM (*85*)—showed good survival and neuronal differentiation, indicating that our cell line performs well with lower glucose levels. Further investigation

into how medium composition affects hNPC behaviour would be valuable for continued use of this cell line.

4.3 EFFECTS OF SUBSTRATE TOPOGRAPHY ON NUCLEUS MORPHOLOGY AND ALIGNMENT

We demonstrate that hNPCs on random fibrous scaffold have nuclei with significantly shorter elongations compared to those of hNPCs cultured on flat glass slides or aligned fibres. Furthermore, nuclei on aligned fibres are quite consistently more elongated than those on flat surfaces, but not significantly. Nucleus morphology has been linked to gene expression for certain cell lines (*35*); it would be interesting to investigate if the same is true for hNPCs, which is why such studies are on-going in our laboratory using microarrays. Over time, most groups exhibited increased elongation and neuronal differentiation, and future research could be done to examine whether there exists a connection between these two observations. However, as will be discussed below, inhibition of myosin II led to a decrease in elongation, and possibly an increase in neuronal differentiation fate, which would not be in line with this hypothesis.

Not very surprisingly, the nuclei tend to align with the topographical features of the substrate. We demonstrate significantly higher alignment of nuclei grown on aligned fibres compared to those grown on isotropic surfaces. Neural alignment to topographical features has been previously observed in a number of studies (*25*, *89*, *90*) and has implications in cell migration (*50*) and may also influence phenotypic differentiation fate of stem cells (*47*). Our results do not indicate any connection between nucleus alignment and differentiation, but this should be further investigated using better experimental methods.

4.4 EFFECTS OF MYOSIN II INHIBITION

We had hoped to use myosin II inhibition to study mechanotransductory pathways responsible for topographical effects on differentiation of hNPCs. However, as no significant differences in differentiation were found between groups on glass slides and fibrous scaffolds in project A, and due to poor viability of cells on fibrous scaffolds in project B, no conclusions can be drawn. However, we can still examine the effects of myosin II inhibition on cells grown on glass slides.

Using phase contrast microscopy during culture we observed that the addition of blebbistatin to hNPC cultures led to thinner outgrowths of cell, and less flat appearances compared to both negative and vehicular controls. Furthermore, we observed that blebbistatin-treated group had lower cell density than the two control groups. Finally, the two control groups, but not the blebbistatin-treated group, started exhibiting circular areas devoid of cells in the last days of culture. These circular areas appeared to form a sort of hexagonal pattern which has previously been

observed with the same cell line as well as with induced pluripotent stem cells (personal communication with Ulrica Englund-Johansson). Since blebbistatin affects cytoskeletal contractility, effects on cell morphology are not surprising; however, the reasons for lower cell density and lack of empty circular areas are unclear. Possible explanations include potential effects on mitosis, cell survival, migration and cell-cell adhesion, but more research is needed to ascertain the true reasons.

Both blebbistatin and, albeit less prominently, vehicular control seemed to increase neuronal differentiation compared to negative control, as seen by the increase in fraction of MAP2+ cells (and decrease in SOX2+ cells); however the spread of data points is rather large and only one biological replicate was examined, making the strength of these results rather weak. Differences in nucleus elongation between blebbistatin-treated groups and the control groups were visible, with those of the former being noticeably shorter. This may indicate the role of actomyosin contractility for conveying topographical cues to the nuclear envelope. Future experiments to examine whether myosin II inhibition has an effect on nucleus alignments would be interesting.

4.5 ETHICAL ISSUES

Research using stem cells, and especially human embryonic stem cells, is associated with ethical concerns and controversies (*91*). Many of these concerns arise from beliefs that life starts at conception and that embryos thus should share the same moral rights as adults. A more prevalent view in the scientific community is that embryos, although not human beings, can be considered *potential* human beings and thus need to be handled with respect; as such, their use for stem cells must be justified by the aims of the research (*91*). A benefit with the cell line used in this thesis is its mitotic capacity: the progenitor cells can be expanded with exponential growth (*59*) and can be frozen for later; consequently progenitors from a single embryo can be used for a vast amount of experiments, with potential for contributing to the improvement of quality of life for countless patients worldwide.

Another ethical issue, which is common for almost all biomedical research, is the use of animals. In this thesis, we have studied cell culture on fibrous scaffolds, and have not used any animal models; furthermore, one of the promising uses of fibrous scaffolds is the ability to mimic *in vivo* microenvironments and thus they hold potential to reduce the need of animal models for disease research and drug development in the future. Nevertheless, *in vitro* research requires animals for obtaining antibodies, proteins and other biological material. One ingredient used in our experiments which has attracted a great deal of concern is FBS, the extraction of which causes suffering for the fetal calf (*92*). More humane alternatives for FBS media are available and include donor horse serum-based media (*93*) and serum-free media (*61*).

4.6 CONCLUSIONS AND OUTLOOK

The main findings of this thesis are presented below:

1. We show no significant differences in overall differentiation capacity, or phenotypic fate between hNPCs seeded on glass slides and electrospun fibrous scaffolds.

2. We show that hNPCs tend to align with the topographical features of the substrate, with significant differences in nucleus alignment between cells on aligned fibrous scaffolds and those cultured on glass slides or random fibres.

Electrospun fibrous scaffolds and hNPCs are promising for use in regenerative therapies and *in vitro* disease modelling. However, much research still needs to be done in order to obtain more consistent results. More specifically, potential differences in overall differentiation capacity between different passages of hNPCs must be surveyed; the effects of medium composition should be examined, and here I would advocate the use of chemically defined media; finally, the low cell survival on random fibrous scaffolds should be investigated. Nevertheless, continued research in this field will certainly generate important results for the progress of neuroregenerative medicine and *in vitro* modelling of neurological diseases.

References

(*1*) Hussain, R., Zubair, H., Pursell, S., and Shahab, M. (2018). Neurodegenerative Diseases: Regenerative Mechanisms and Novel Therapeutic Approaches. *Brain Sciences 8*, 177.

(*2*) Duval, K., Grover, H., Han, L.-H., Mou, Y., Pegoraro, A. F., Fredberg, J., and Chen, Z. (2017). Modeling Physiological Events in 2D vs. 3D Cell Culture. *Physiology 32*, 266–277.

(*3*) Edmondson, R., Broglie, J. J., Adcock, A. F., and Yang, L. (2014). Three-Dimensional Cell Culture Systems and Their Applications in Drug Discovery and Cell-Based Biosensors. *Assay and Drug Development Technologies 12*, 207–218.

(*4*) Baker, B. M., and Chen, C. S. (2012). Deconstructing the third dimension – how 3D culture microenvironments alter cellular cues. *Journal of Cell Science 125*, 3015–3024.

(*5*) Hopkins, A. M., DeSimone, E., Chwalek, K., and Kaplan, D. L. (2015). 3D in vitro modeling of the central nervous system. *Progress in Neurobiology 125*, 1–25.

(*6*) Tam, R. Y., Fuehrmann, T., Mitrousis, N., and Shoichet, M. S. (2014). Regenerative Therapies for Central Nervous System Diseases: a Biomaterials Approach. *Neuropsychopharmacology 39*, 169–188.

(*7*) Bang, O. Y., Lee, J. S., Lee, P. H., and Lee, G. (2005). Autologous mesenchymal stem cell transplantation in stroke patients. *Annals of Neurology 57*, 874–882.

(*8*) Modo, M. (2019). Bioscaffold-Induced Brain Tissue Regeneration. *Frontiers in Neuroscience 13*, 1156.

(*9*) Adil, M. M., Vazin, T., Ananthanarayanan, B., Rodrigues, G. M. C., Rao, A. T., Kulkarni, R. U., Miller, E. W., Kumar, S., and Schaffer, D. V. (2017). Engineered hydrogels increase the post-transplantation survival of encapsulated hESC-derived midbrain dopaminergic neurons. *Biomaterials 136*, 1–11.

(*10*) Zhong, J., Chan, A., Morad, L., Kornblum, H. I., Fan, G., and Carmichael, S. T. (2010). Hydrogel Matrix to Support Stem Cell Survival After Brain Transplantation in Stroke. *Neurorehabilitation and Neural Repair 24*, 636–644.

(*11*) Reichardt, L., and Prokop, A. (2011). Introduction: The role of extracellular matrix in nervous system development and maintenance. *Developmental Neurobiology 71*, 883–888.

(*12*) Xiao, N., and Le, Q.-T. (2016). Neurotrophic Factors and Their Potential Applications in Tissue Regeneration. *Archivum Immunologiae et Therapiae Experimentalis 64*, 89–99.

(*13*) Reilly, G. C., and Engler, A. J. (2010). Intrinsic extracellular matrix properties regulate stem cell differentiation. *Journal of Biomechanics 43*, 55–62.

(*14*) Rowlands, A. S., George, P. A., and Cooper-White, J. J. (2008). Directing osteogenic and myogenic differentiation of MSCs: interplay of stiffness and adhesive ligand presentation. *American Journal of Physiology-Cell Physiology 295*, C1037–C1044.

(*15*) Hersel, U., Dahmen, C., and Kessler, H. (2003). RGD modified polymers: biomaterials for stimulated cell adhesion and beyond. *Biomaterials 24*, 4385–4415.

(*16*) Tashiro, K., Sephel, G. C., Weeks, B., Sasaki, M., Martin, G. R., Kleinman, H. K., and Yamada, Y. (1989). A synthetic peptide containing the IKVAV sequence from the A chain of laminin mediates cell attachment, migration, and neurite outgrowth. *Journal of Biological Chemistry 264*, 16174–16182.

(*17*) Yamada, K. M., and Miyamoto, S. (1995). Integrin transmembrane signaling and cytoskeletal control. *Current Opinion in Cell Biology 7*, 681–689.

(*18*) Kim, S.-H., Turnbull, J., and Guimond, S. (2011). Extracellular matrix and cell signalling: the dynamic cooperation of integrin, proteoglycan and growth factor receptor. *The Journal of Endocrinology 209*, 139–151.

(*19*) Benarroch, E. E. (2015). Extracellular matrix in the CNS: Dynamic structure and clinical correlations. *Neurology 85*, 1417–1427.

(*20*) Zimmermann, D. R., and Dours-Zimmermann, M. T. (2008). Extracellular matrix of the central nervous system: from neglect to challenge. *Histochemistry and Cell Biology 130*, 635–653.

(*21*) Letourneau, P. In *Encyclopedia of Neuroscience*, Squire, L. R., Ed.; Academic Press: Oxford, 2009, pp 1139–1145.

(*22*) Engler, A. J., Sen, S., Sweeney, H. L., and Discher, D. E. (2006). Matrix Elasticity Directs Stem Cell Lineage Specification. *Cell 126*, 677–689.

(*23*) Leipzig, N. D., and Shoichet, M. S. (2009). The effect of substrate stiffness on adult neural stem cell behavior. *Biomaterials 30*, 6867–6878.

(*24*) Young, J. L., Holle, A. W., and Spatz, J. P. (2016). Nanoscale and mechanical properties of the physiological cell–ECM microenvironment. *Experimental Cell Research 343*, 3–6.

(*25*) Lim, S. H., Liu, X. Y., Song, H., Yarema, K. J., and Mao, H.-Q. (2010). The effect of nanofiber-guided cell alignment on the preferential differentiation of neural stem cells. *Biomaterials 31*, 9031–9039.

(*26*) Yang, F., Murugan, R., Wang, S., and Ramakrishna, S. (2005). Electrospinning of nano/micro scale poly(l-lactic acid) aligned fibers and their potential in neural tissue engineering. *Biomaterials 26*, 2603–2610.

(*27*) Chen, C. S., Mrksich, M., Huang, S., Whitesides, G. M., and Ingber, D. E. (1997). Geometric Control of Cell Life and Death. *Science 276*, 1425–1428.

(*28*) Dalby, M. J., Riehle, M. O., Yarwood, S. J., Wilkinson, C. D. W., and Curtis, A. S. G. (2003). Nucleus alignment and cell signaling in fibroblasts: response to a micro-grooved topography. *Experimental Cell Research 284*, 272–280.

(*29*) Teo, B. K. K., Ankam, S., Chan, L. Y., and Yim, E. K. F. In *Methods in Cell Biology*, Shivashankar, G. V., Ed.; Nuclear Mechanics & Genome Regulation, Vol. 98; Academic Press: 2010, pp 241–294.

(*30*) Jansen, K. A., Atherton, P., and Ballestrem, C. (2017). Mechanotransduction at the cell-matrix interface. *Seminars in Cell & Developmental Biology 71*, 75–83.

(*31*) Wolfenson, H., Yang, B., and Sheetz, M. P. (2019). Steps in Mechanotransduction Pathways that Control Cell Morphology. *Annual Review of Physiology 81*, 585–605.

(*32*) Wolfenson, H., Lavelin, I., and Geiger, B. (2013). Dynamic Regulation of the Structure and Functions of Integrin Adhesions. *Developmental Cell 24*, 447–458.

(*33*) Hu, X., Jing, C., Xu, X., Nakazawa, N., Cornish, V. W., Margadant, F. M., and Sheetz, M. P. (2016). Cooperative Vinculin Binding to Talin Mapped by Time-Resolved Super Resolution Microscopy. *Nano Letters 16*, 4062–4068.

(*34*) Cho, S., Irianto, J., and Discher, D. E. (2017). Mechanosensing by the nucleus: From pathways to scaling relationships. *Journal of Cell Biology 216*, 305–315.

(*35*) Thomas, C. H., Collier, J. H., Sfeir, C. S., and Healy, K. E. (2002). Engineering gene expression and protein synthesis by modulation of nuclear shape. *Proceedings of the National Academy of Sciences 99*, 1972–1977.

(*36*) Straight, A. F., Cheung, A., Limouze, J., Chen, I., Westwood, N. J., Sellers, J. R., and Mitchison, T. J. (2003). Dissecting Temporal and Spatial Control of Cytokinesis with a Myosin II Inhibitor. *Science 299*, 1743–1747.

(*37*) Wang, Y., Tan, H., and Hui, X. (2018). Biomaterial Scaffolds in Regenerative Therapy of the Central Nervous System. *BioMed Research International 2018*, 7848901.

(*38*) Hong, J., Yeo, M., Yang, G. H., and Kim, G. (2019). Cell-Electrospinning and Its Application for Tissue Engineering. *International Journal of Molecular Sciences 20*, 6208.

(*39*) Tucker, N., Stanger, J. J., Staiger, M. P., Razzaq, H., and Hofman, K. (2012). The History of the Science and Technology of Electrospinning from 1600 to 1995. *Journal of Engineered Fibers and Fabrics 7*, 63–73.

(*40*) Xue, J., Wu, T., Dai, Y., and Xia, Y. (2019). Electrospinning and Electrospun Nanofibers: Methods, Materials, and Applications. *Chemical Reviews 119*, 5298–5415.

(*41*) Matthews, J. A., Wnek, G. E., Simpson, D. G., and Bowlin, G. L. (2002). Electrospinning of Collagen Nanofibers. *Biomacromolecules 3*, 232–238.

(*42*) Ji, Y., Ghosh, K., Shu, X. Z., Li, B., Sokolov, J. C., Prestwich, G. D., Clark, R. A. F., and Rafailovich, M. H. (2006). Electrospun three-dimensional hyaluronic acid nanofibrous scaffolds. *Biomaterials 27*, 3782–3792.

(*43*) Jin, H.-J., Chen, J., Karageorgiou, V., Altman, G. H., and Kaplan, D. L. (2004). Human bone marrow stromal cell responses on electrospun silk fibroin mats. *Biomaterials 25*, 1039–1047.

(*44*) Chong, E. J., Phan, T. T., Lim, I. J., Zhang, Y. Z., Bay, B. H., Ramakrishna, S., and Lim, C. T. (2007). Evaluation of electrospun PCL/gelatin nanofibrous scaffold for wound healing and layered dermal reconstitution. *Acta Biomaterialia 3*, 321–330.

(*45*) Yin, A., Zhang, K., McClure, M. J., Huang, C., Wu, J., Fang, J., Mo, X., Bowlin, G. L., Al-Deyab, S. S., and El-Newehy, M. (2013). Electrospinning collagen/chitosan/poly(L-lactic acid-co-□-caprolactone) to form a vascular graft: Mechanical and biological characterization. *Journal of Biomedical Materials Research Part A 101A*, 1292–1301.

(*46*) Chew, S. Y., Wen, J., Yim, E. K. F., and Leong, K. W. (2005). Sustained Release of Proteins from Electrospun Biodegradable Fibers. *Biomacromolecules 6*, 2017–2024.

(*47*) Jiang, X., Cao, H. Q., Shi, L. Y., Ng, S. Y., Stanton, L. W., and Chew, S. Y. (2012). Nanofiber topography and sustained biochemical signaling enhance human mesenchymal stem cell neural commitment. *Acta Biomaterialia 8*, 1290–1302.

(*48*) Lim, S. H., and Mao, H.-Q. (2009). Electrospun scaffolds for stem cell engineering. *Advanced Drug Delivery Reviews 61*, 1084–1096.

(*49*) Jakobsson, A., Ottosson, M., Zalis, M. C., O'Carroll, D., Johansson, U. E., and Johansson, F. (2017). Three-dimensional functional human neuronal networks in uncompressed low-density electrospun fiber scaffolds. *Nanomedicine: Nanotechnology, Biology and Medicine 13*, 1563–1573.

(*50*) Englund-Johansson, U., Netanyah, E., and Johansson, F. (2017). Tailor-Made Electrospun Culture Scaffolds Control Human Neural Progenitor Cell Behavior—Studies on Cellular Migration and Phenotypic Differentiation. *Journal of Biomaterials and Nanobiotechnology 08*, 1–21.

(*51*) Crapo, P. M., Medberry, C. J., Reing, J. E., Tottey, S., van der Merwe, Y., Jones, K. E., and Badylak, S. F. (2012). Biologic scaffolds composed of central nervous system extracellular matrix. *Biomaterials 33*, 3539–3547.

(*52*) Drury, J. L., and Mooney, D. J. (2003). Hydrogels for tissue engineering: scaffold design variables and applications. *Biomaterials 24*, 4337–4351.

(*53*) Caliari, S. R., and Burdick, J. A. (2016). A practical guide to hydrogels for cell culture. *Nature Methods 13*, 405–414.

(*54*) Martínez-Cerdeño, V., and Noctor, S. C. (2018). Neural Progenitor Cell Terminology. *Frontiers in Neuroanatomy 12*, 104.

(*55*) Seaberg, R. M., and van der Kooy, D. (2003). Stem and progenitor cells: the premature desertion of rigorous definitions. *Trends in Neurosciences 26*, 125–131.

(*56*) Reynolds, B. A., and Weiss, S. (1992). Generation of Neurons and Astrocytes from Isolated Cells of the Adult Mammalian Central Nervous System. *Science 255*, 1707–1710.

(*57*) Deleyrolle, L. P., and Reynolds, B. A. In *Neural Cell Transplantation: Methods and Protocols*, Gordon, D., and Scolding, N. J., Eds.; Methods in Molecular Biology; Humana Press: Totowa, NJ, 2009, pp 91–101.

(*58*) Ge, D., Song, K., Guan, S., Dai, M., Ma, X., Liu, T., and Cui, Z. (2012). Effect of the neurosphere size on the viability and metabolism of neural stem/progenitor cells. *African Journal of Biotechnology 11*, 3976–3985.

(*59*) Carpenter, M. K., Cui, X., Hu, Z.-y., Jackson, J., Sherman, S., Seiger, Å., and Wahlberg, L. U. (1999). In Vitro Expansion of a Multipotent Population of Human Neural Progenitor Cells. *Experimental Neurology 158*, 265–278.

(*60*) Spivak-Kroizman, T., Lemmon, M. A., Dikic, I., Ladbury, J. E., Pinchasi, D., Huang, J., Jaye, M., Crumley, G., Schlessinger, J., and Lax, I. (1994). Heparin-induced oligomerization of FGF molecules is responsible for FGF receptor dimerization, activation, and cell proliferation. *Cell 79*, 1015–1024.

(*61*) van der Valk, J., Brunner, D., De Smet, K., Fex Svenningsen, Å., Honegger, P., Knudsen, L. E., Lindl, T., Noraberg, J., Price, A., Scarino, M. L., and Gstraunthaler, G. (2010). Optimization of chemically defined cell culture media – Replacing fetal bovine serum in mammalian in vitro methods. *Toxicology in Vitro 24*, 1053–1063.

(*62*) Rampersad, S. N. (2012). Multiple Applications of Alamar Blue as an Indicator of Metabolic Function and Cellular Health in Cell Viability Bioassays. *Sensors 12*, 12347–12360.

(*63*) Burry, R. W., *Immunocytochemistry: A Practical Guide for Biomedical Research*; Springer-Verlag: New York, 2010.

(*64*) Gubbay, J., Collignon, J., Koopman, P., Capel, B., Economou, A., Münsterberg, A., Vivian, N., Goodfellow, P., and Lovell-Badge, R. (1990). A gene mapping to the sex-determining region of the mouse Y chromosome is a member of a novel family of embryonically expressed genes. *Nature 346*, 245–250.

(*65*) Dailey, L., Yuan, H., and Basilico, C. (1994). Interaction between a novel F9-specific factor and octamer-binding proteins is required for cell-type-restricted activity of the fibroblast growth factor 4 enhancer. *Molecular and Cellular Biology 14*, 7758–7769.

(*66*) Graham, V., Khudyakov, J., Ellis, P., and Pevny, L. (2003). SOX2 Functions to Maintain Neural Progenitor Identity. *Neuron 39*, 749–765.

(*67*) Eng, L. F. (1985). Glial fibrillary acidic protein (GFAP): the major protein of glial intermediate filaments in differentiated astrocytes. *Journal of Neuroimmunology 8*, 203–214.

(*68*) Liu, Y., Namba, T., Liu, J., Suzuki, R., Shioda, S., and Seki, T. (2010). Glial fibrillary acidic protein-expressing neural progenitors give rise to immature neurons via early intermediate progenitors expressing both glial fibrillary acidic protein and neuronal markers in the adult hippocampus. *Neuroscience 166*, 241–251.

(*69*) Katsetos, C. D., Legido, A., Perentes, E., and Mörk, S. J. (2003). Class III β-Tubulin Isotype: A Key Cytoskeletal Protein at the Crossroads of Developmental Neurobiology and Tumor Neuropathology. *Journal of Child Neurology 18*, 851–866.

(*70*) Dráberová, E., Del Valle, L., Gordon, J., Marková, V., Šmejkalová, B., Bertrand, L., de Chadarévian, J.-P., Agamanolis, D. P., Legido, A., Khalili, K., Dráber, P., and Katsetos, C. D. (2008). Class III β-Tubulin Is Constitutively Coexpressed With Glial Fibrillary Acidic Protein and Nestin in Midgestational Human Fetal Astrocytes: Implications for Phenotypic Identity. *Journal of Neuropathology & Experimental Neurology 67*, 341–354.

(*71*) Katsetos, C. D. et al. (2001). Aberrant Localization of the Neuronal Class III β-Tubulin in Astrocytomas. *Archives of Pathology & Laboratory Medicine 125*, 613–624.

(*72*) Cassimeris, L., and Spittle, C. In *International Review of Cytology*; Academic Press: 2001; Vol. 210, pp 163–226.

(*73*) Garner, C. C., Brugg, B., and Matus, A. (1988). A 70-Kilodalton Microtubule-Associated Protein (MAP2c), Related to MAP2. *Journal of Neurochemistry 50*, 609–615.

(*74*) Rosser, A. E., Tyers, P., ter Borg, M., Dunnett, S. B., and Svendsen, C. N. (1997). Co-expression of MAP-2 and GFAP in cells developing from rat EGF responsive precursor cells. *Developmental Brain Research 98*, 291–295.

(*75*) Svendsen, C. N., Bhattacharyya, A., and Tai, Y.-T. (2001). Neurons from stem cells: preventing an identity crisis. *Nature Reviews Neuroscience 2*, 831–834.

(*76*) van der Walt, S., Schönberger, J. L., Nunez-Iglesias, J., Boulogne, F., Warner, J. D., Yager, N., Gouillart, E., Yu, T., and contributors the scikit-image, t. s.-i. (2014). scikit-image: image processing in Python. *PeerJ 2*, e453.

(*77*) Bradski, G. (2000). The OpenCV Library. *Dr. Dobb's Journal of Software Tools*.

(*78*) van der Walt, S., Colbert, S. C., and Varoquaux, G. (2011). The NumPy Array: A Structure for Efficient Numerical Computation. *Computing in Science Engineering 13*, 22–30.

(*79*) Virtanen, P. et al. (2020). SciPy 1.0: fundamental algorithms for scientific computing in Python. *Nature Methods 17*, 261–272.

(*80*) Seabold, S., and Perktold, J. In *9th Python in Science Conference*, 2010.

(*81*) Hunter, J. D. (2007). Matplotlib: A 2D Graphics Environment. *Computing in Science Engineering 9*, 90–95.

(*82*) Davidson, P., Bigerelle, M., Bounichane, B., Giazzon, M., and Anselme, K. (2010). Definition of a simple statistical parameter for the quantification of orientation in two dimensions: Application to cells on grooves of nanometric depths. *Acta Biomaterialia 6*, 2590–2598.

(*83*) Yang, P., M. Baker, R., H. Henderson, J., and T. Mather, P. (2013). In vitro wrinkle formation via shape memory dynamically aligns adherent cells. *Soft Matter 9*, 4705–4714.

(*84*) Jayme, D. W., Epstein, D. A., and Conrad, D. R. (1988). Fetal bovine serum alternatives. *Nature 334*, 547–548.

(*85*) Bardy, C. et al. (2015). Neuronal medium that supports basic synaptic functions and activity of human neurons in vitro. *Proceedings of the National Academy of Sciences of the United States of America 112*, E2725–E2734.

(*86*) Goyal, M. S., and Raichle, M. E. (2018). Glucose requirements of the developing human brain. *Journal of pediatric gastroenterology and nutrition 66*, S46–S49.

(*87*) Chen, X., Shen, W.-B., Yang, P., Dong, D., Sun, W., and Yang, P. (2018). High Glucose Inhibits Neural Stem Cell Differentiation Through Oxidative Stress and Endoplasmic Reticulum Stress. *Stem Cells and Development 27*, 745–755.

(*88*) Fusco, S., Leone, L., Barbati, S. A., Samengo, D., Piacentini, R., Maulucci, G., Toietta, G., Spinelli, M., McBurney, M., Pani, G., and Grassi, C. (2016). A CREB-Sirt1-Hes1 Circuitry Mediates Neural Stem Cell Response to Glucose Availability. *Cell Reports 14*, 1195–1205.

(*89*) Marcus, M., Baranes, K., Park, M., Choi, I. S., Kang, K., and Shefi, O. (2017). Interactions of Neurons with Physical Environments. *Advanced Healthcare Materials 6*, 1700267.

(*90*) Leach, M. K., Feng, Z.-Q., Gertz, C. C., Tuck, S. J., Regan, T. M., Naim, Y., Vincent, A. M., and Corey, J. M. (2011). The Culture of Primary Motor and Sensory Neurons in Defined Media on Electrospun Poly-L-lactide Nanofiber Scaffolds. *JoVE (Journal of Visualized Experiments)*, e2389.

(*91*) Lo, B., and Parham, L. (2009). Ethical Issues in Stem Cell Research. *Endocrine Reviews 30*, 204–213.

(*92*) van der Valk, J., Mellor, D., Brands, R., Fischer, R., Gruber, F., Gstraunthaler, G., Hellebrekers, L., Hyllner, J., Jonker, F. H., Prieto, P., Thalen, M., and Baumans, V. (2004). The humane collection of fetal bovine serum and possibilities for serum-free cell and tissue culture. *Toxicology in Vitro 18*, 1–12.

(*93*) Malakpour Permlid, A., Roci, P., Fredlund, E., Fält, F., Önell, E., Johansson, F., and Oredsson, S. (2019). Unique animal friendly 3D culturing of human cancer and normal cells. *Toxicology in Vitro 60*, 51–60.

Appendix A
Blebbistatin Pilot Projects

PILOT 1

Aim The aim of the first pilot study was to investigate the toxicity of blebbistatin and its vehicle DMSO, and find an optimal concentration where myosin is noticeably inhibited, but the cell viability is not adversely affected. Two different concentrations, 1 µM and 20 µM, of blebbistatin were examined. The blebbistatin was dissolved in DMSO and thus two control groups with the corresponding concentrations of DMSO were used for comparison.

Methods Passage 12-13 hNPCs were seeded onto PLL-coated glass slides in a 24-well plate, with a cell count of 100 000 per well. The cells were cultured in 1 % FBS medium for a total of 20 DIV, replacing the medium every other day. Starting at 1 DIV, the respective chemicals were added to their corresponding wells when replacing the medium. Cell morphologies were photographed using a phase contrast microscope before each medium exchange. At 20 DIV, an Alamar Blue cell viability assay was conducted and thereafter the cells were fixed with 4 % PFA.

Results Phase contrast microscopy on day 1 *in vitro* – before the addition of the respective chemicals to the media – revealed similar morphologies for all groups. However, many wells showed an uneven spread and number of cells, with very few cells in some wells. At 3 DIV, the cells treated with blebbistatin appear to have thinner outgrowths, but no quantitative analysis was done. At higher DIVs the cells of many wells have multiplied in numbers and started forming larger dense clusters and the morphology differences were less noticeable. For the higher blebbistatin and DMSO concentrations, the number of cells was decreasing and traces of cell death were visible. At 20 DIV before the termination of the experiment, the number of cells per well was more polarized: the cells had either multiplied several times or had almost completely died. The results of the Alamar Blue viability assay performed at 20 DIV are displayed in Figure A.1; the results show similar viability for the untreated group and the 0.1 % DMSO group. Both the 20 µM blebbistatin and 2 % DMSO groups have very low viabilities, similar to that of the control group without any cells.

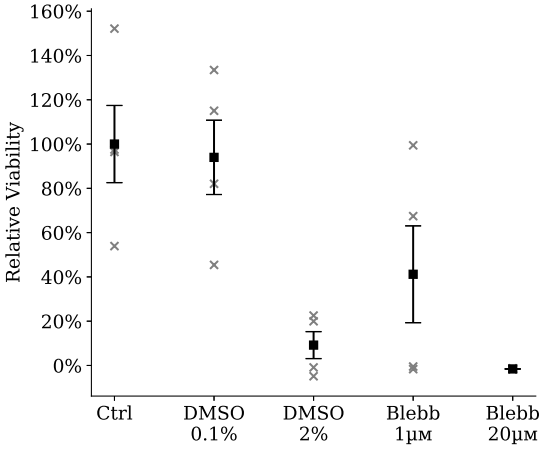

Figure A.1. Results of the Alamar Blue viability assay at 20 DIV. Results are displayed as measurements and mean±SEM. The control group to the left was a sample of medium without cells

Discussion The results indicate that the cells treated with 20 µM blebbistatin or 2 % DMSO have poor viability over time; this is probably due to the high concentration of DMSO, which is above recommended levels for cell culture. The large spread of viability in the 1 µM blebbistatin group can likely be explained by poor cell seeding; before treating the group with blebbistatin it was noted that the cell count was low in two of the wells. In conclusion, both 1 µM and 20 µM blebbistatin seem to cause a noticeable change in morphology after 3 DIV, but after this time the effect is less noticeable. Furthermore, 2 % DMSO seems to be toxic to the cells and thus it is difficult to examine the effect of 20 µM

blebbistatin over longer times. For a next experiment, using less diluted blebbistatin would be suitable, more concentrations should be studied, and cell seeding technique must be improved.

PILOT 2

Aim and Scope The aim of the second pilot study was to further investigate how different concentrations of blebbistatin affect cell morphology and viability; we examined the effects of three different concentrations: 1 µM, 5 µM, and 10 µM and correpsonding control groups. We cultured the seeded cells for 10 DIV instead of 20 DIV as in the first pilot, since we had observed that morphology differences of the different groups were visible already after a few days. In this pilot, we examined cell morphology using phase contrast microscopy, we examined differentiation using ICC with SOX2 and MAP2 as markers, and we assessed viabilities using an Alamar Blue assay. We intended to include Western blotting as an additional means to study differentiation markers, but our protein concentrations were too low to finalize this plan.

Methods Passage 14-15 hNPCs were seeded onto PLL-coated glass slides with a concentration of around 75 000 cm^{-2}. All groups were cultured in 1 % FBS medium, with the respective chemicals added with every medium exchange from 1 DIV and on. Morphologies were documented at 1, 3, 6 and 9 DIV. At 10 DIV, the viabilities were examined in an Alamar blue viability assay, and the cells were subsequently fixed with 4 % PFA. Cells intended for Western blot analysis were trypsinated, and lysed using RIPA buffer at 11 DIV; protein concentrations were thereafter measured in a Pierce Rapid Gold BCA Protein Assay.

Results Morphology differences between the 5 µM, 10 µM and their control groups were noticed after a few hours after the addition of the respective chemicals to the cultures, and were persistent throughout the culture until fixation. The 1 µM group showed smaller differences with its control group. Quantification of cell morphologies was performed (data not shown) and indicated a larger proportion of unipolar or multipolar cells with long processes for the cells treated with blebbistatin. For the control groups, smaller round cells or large flat cells were more common.

The Alamar Blue assay (Figure A.2) indicated differences in viability for the different groups, with the group treated with the highest DMSO concentration surprisingly exhibiting the highest viability. Many of the low viability measurements correspond to wells in which we had seen a low cell count since 1 DIV.

The cell counting showed high expression of SOX2, with no significant difference between any groups. Furthermore, all cells expressed MAP2, but none were similar to the type of expression seen in project A, indicating a lack of differentiation into neurons. In light of these results, and the low protein concentrations following the RIPA lysis, we deemed it fruitless to continue with a Western blot analysis.

Discussion The DMSO concentrations in this pilot do not seem to have any toxic effect on the cells; instead we can attribute the low viabilities of certain groups to poor seeding consistency and possibly to toxic effects of blebbistatin. Nevertheless, as the 5 µM blebbistatin group showed clear differences in cell morphology, and higher viability than the 10 µM group, we chose to continue with this concentration for our next experiments. As we saw no clear differentiation to mature neurons after 10 DIV we will revert to a culture time of 20 DIV, and to increase cell density, differentiation and viability, we will seed the wells with a higher number of cells.

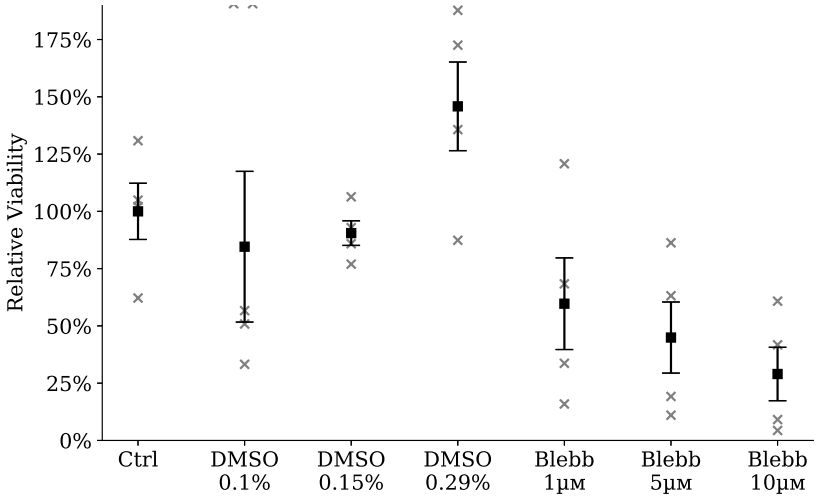

Figure A.2. Results of the Alamar Blue viability assay at 10DIV $n = 4$ wells were analyzed per group. Each data point represents the viability of a single well, normalized to the average of the control group, and is presented along with mean±SEM for each group.

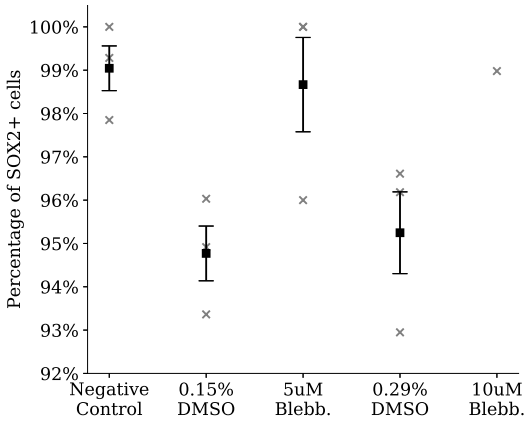

Figure A.3. Quantification of SOX2+ cells at 10 DIV. The mean of each well and group is displayed as a data point; the mean±SEM for these point is also shown. $n = 3$ technical replicates for each group except 10 µM blebbistatin, where cell count was too low for quantification. The results reveal overall high expression of SOX2 indicating low differentiation.

Appendix B

Additional Photo Montages

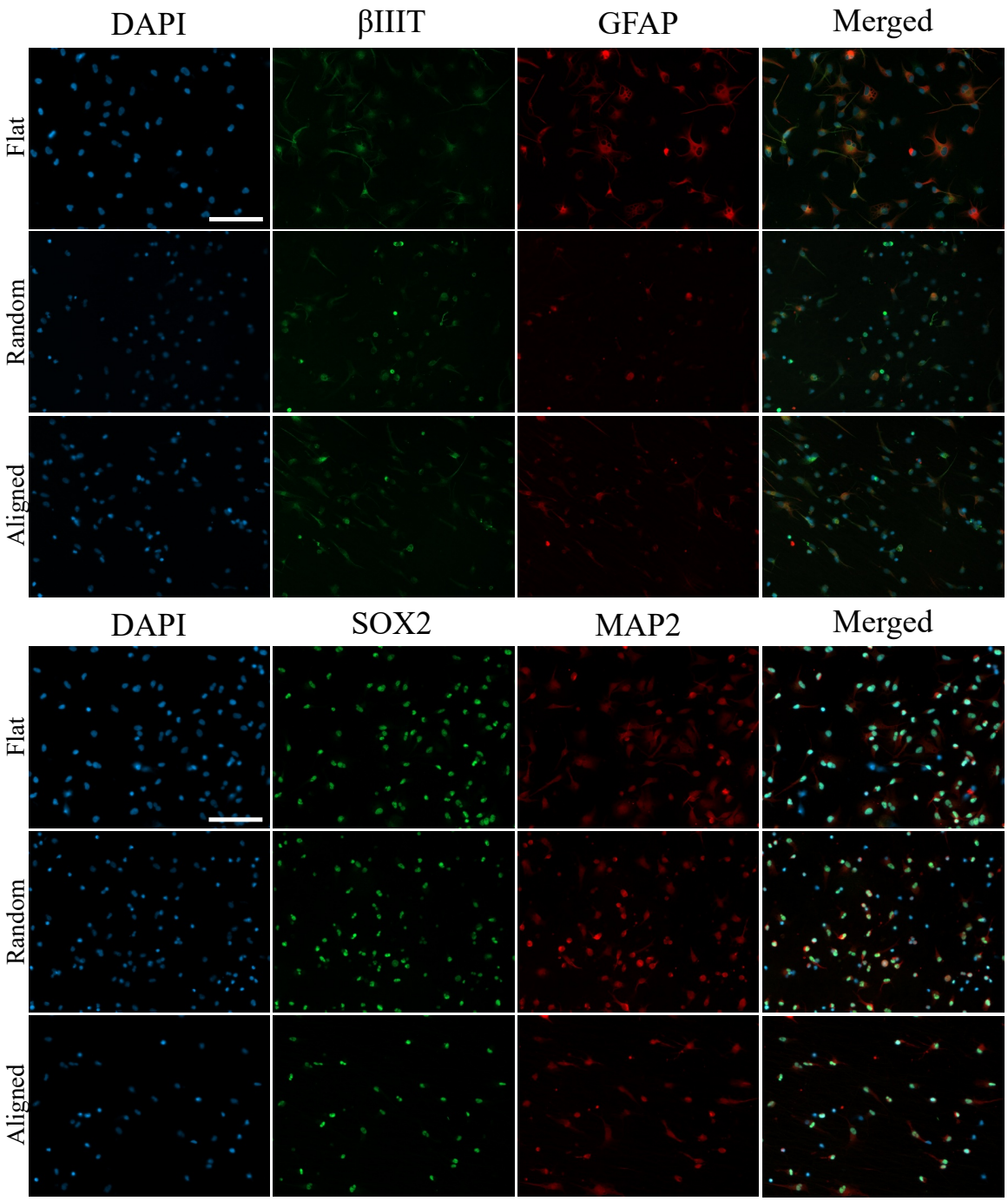

Figure B.1. Fluorescence microscopy images of the different groups in project A at 0 DIV. Notice the presence of cells which are neither SOX2+ or MAP2+. Scale bars are 100 μm.

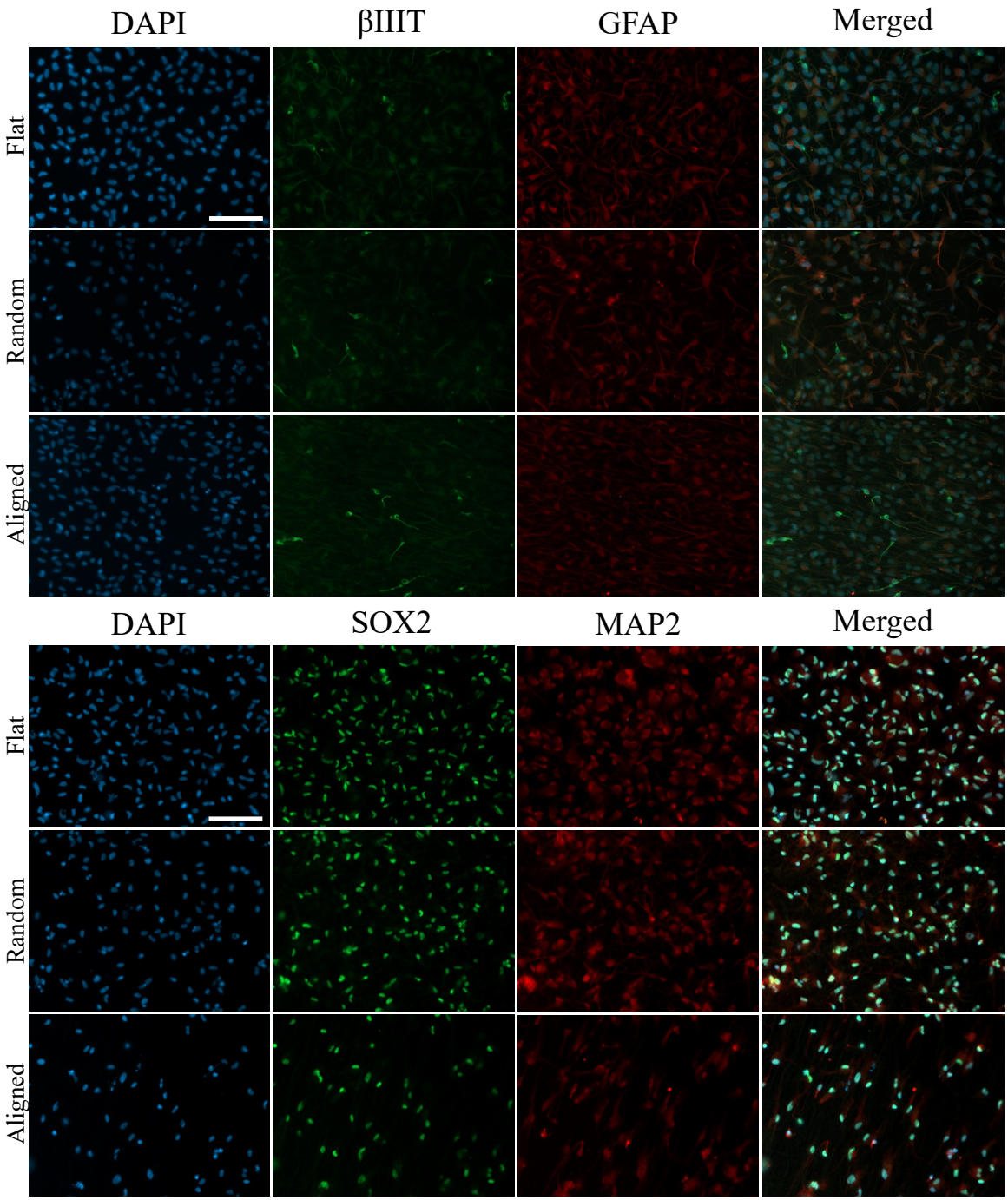

Figure B.2. Fluorescence microscopy images of the different groups in project A at 10 DIV. Cell numbers have increased since 0 DIV, and morphologies have changed. Notice the presence of clear neuronal differentiation in the βIIIT staining. Scale bars are 100 μm.

Appendix C
Protocols and Recipes

CULTURE MEDIUM RECIPES

Basic medium and complete (expansion) medium were prepared according to the recipes below. Differentiation medium was prepared by adding 1 % FBS to basic medium. All media were filtered with a 0.2 µm filter after preparation. Basic medium should be used within one month, complete medium and differentiation medium within one week.

Basic Medium

Ingredients	50 ml	100 ml	500 ml
DMEM/F12 1x *ThermoFisher no 21331-020*	47 ml	94 ml	470 ml
N-2 Supplement *ThermoFisher no 17502-001*	0.5 ml	1 ml	5 ml
L-Glutamine P/S (Stock 200 mM, 10000 units /ml Penicillin, 10 000 µg/ml streptomycin) *ThermoFisher no 10378016*	0.5 ml	1 ml	5 ml
Glucose 0.6 % (Stock 30 %) *Sigma no G70213*	1 ml	2 ml	10 ml
Heparin 2 µg/ml (Stock 10 mg/100 ml) *Sigma no H3149*	1 ml	2 ml	10 ml

Complete Medium

Ingredients	50 ml	100 ml	500 ml
Basic Medium	50 ml	100 ml	500 ml
EGF, rec. human EGF (20 ng/ml, stock: 100 µg/ml) *Prospec, CYT-217*	10 µl	20 µl	100 µl
bFGF, rec. basic human FGF (20 ng/ml, stock: 100 µg/ml) *Prospec, CYT-218*	10 µl	20 µl	100 µl
LIF, rec. human LIF (10 ng/ml, stock: 10 µg/ml) Sigma, no L5283 *Prospec CYT-644*	50 µl	100 µl	500 µl

THAWING AND EXPANSION OF HNPCS

1. Get frozen cells in the cryovials in dry ice
2. Prepare 50 ml tubes for every 2 cryovials of the same batch and add 7 ml to 10 ml of basic medium.
3. Quick thaw the cryovials in a 37 °C water bath.
4. Add 1 ml of basic medium to the cells to dilute the freezing medium, as DMSO is toxic to the cells and immediately transfer the content to the rest of the basic medium in the 50 ml tube.
5. Centrifuge at 300g for 5 min.
6. Aspirate supernatant and resuspend the pellet in 2 ml expansion medium.
7. Transfer the cells into a T75 flask containing 18 ml of expansion medium.
8. Check cells under the microscope.
9. Incubate in a cell culture incubator at 37 °C, 5 % CO2, 95 % humidity.
10. Two (2) days after, add 20 ml of fresh expansion medium to each T75 flask and then remove 20 ml of the suspension into a new T75 flask.
11. Incubate in a cell culture incubator at 37 °C, 5 % CO2, 95 % humidity.
12. Feed cells (each flask) with 3 ml to 4 ml every 3rd to 4th day until the neurospheres are big enough and ready for dissociation.

PASSAGING/DISSOCIATION OF HNPCS NEUROSPHERES W. ACCUTASE

1. Transfer content (neurospheres) of T75 flask into a 50 ml tube
2. Centrifuge for 5 min at 1600 rpm
3. Aspirate supernatant and resuspend cell pellet with 5 ml DPBS without Ca++ Mg++
4. Centrifuge for 5 min at 1600 rpm
5. Aspirate supernatant and resuspend cell pellet with 1 ml Accutase.
6. Incubate for 10 min at RT
7. By pipetting up and down, using a 100 µl pipette, dissociate cells until all the neurospheres are in a single cell suspension
8. Add 4 ml of fresh medium to the tube
9. Centrifuge for 5 min at 2000 rpm

10. Aspirate supernatant and resuspend cell pellet with appropriate volume of fresh medium
11. Count the cells using Trypand Blue and TC20 automatic cell counter.
12. Seed according experiment, e.g.:
    (a) Expansion: 2.4M cells in 15 to 20 ml of expansion medium
    (b) Freezing: 4M cells in 15 to 20 ml of expansion medium
    (c) Differentiation: According to experimental setup in differentiation medium

HNPC FREEZING AND THAWING

Medium Preparation

Freeze Medium

Ingredients	5 ml	10 ml	50 ml
Basic medium	4.1 ml	8.25 ml	41.25 ml
DMSO 100 % (final conc. 7.5 %)	0.4 ml	0.75 ml	3.75 ml
BSA (final conc. 10 %)	0.5 g	1 g	5 g

1. Add BSA to basic medium. To dissolve BSA warm the mixture at 37°C water bath. Note: BSA and basic medium can stay for 1 week at 4°C.
2. Add DMSO (just before the freezing).
3. Sterile filter with 0.2 μm filter. (Store at 4°C if not used immediately)

Freezing of Cells

1. Passage as usual and seed them at 4 million per flask
2. Two days after the passage (small spheres) spin down the cells (no passaging!) and add 1ml of freezing medium (approximately 4 million per cryovial) Thus, take one T75 with 4 approx million cells per flask to one cryovial. The numbers will not be exact, but it is not so important here
3. Put the cryovials with cells in a freezing container into -80 degrees for 1-2 days and then finally store at -150°C (liquid nitrogen tank)

IMMUNOSTAINING FOR FIXED CULTURED CELLS

Before starting stainings:

- Prepare blocking solution (PBS + 1 % BSA + 0.25 % Triton X) and have it at RT
- Prepare calculations and solutions with Ab. Note: primary and secondary antibodies diluted in "blocking" solution (1x PBS or TBS + 1 % BSA + 0.25 % Triton X)
- Have 1xPBS or 1 x TBS at RT
- Bring slides/ culture plates with cells from the cold room and keep them at RT (at least 30 min). When at RT, they ready to use.

Note: Be consistent when using the salt buffer (PBS or TBS)

Procedure:

Day 1

1. **Optional:** Pre-incubate samples in blocking solution with 5 % serum for 30 min.
2. Aspirate and add primary antibody solution and incubate for at least 16 h at 4 °C. Remember do not let the cells be without solution for more than 10-15 seconds.

Day 2

1. Collect primary Ab solution and immediately add 1xPBS/ TBS for washing (15 min "incubation")
2. Wash once more (15 min "incubation")
3. Aspirate the washing buffer and add secondary ab solution. Incubate for 1 h (minimum 45 min) at RT in the dark.
4. Collect secondary Ab solution and immediately add 1xPBS/ TBS for washing so that cells don't dry
5. Wash once more
6. Mount using anti-fading media containing DAPI:
   (a) Cultures in **round glass coverslip:**
      i. Add a drop of mounting medium on the glass slide
      ii. With a forcep, carefully pick up the cover slip from the well and place it onto the droplet of mounting medium (avoid bubbles formation). Note to turn the coverslip upside down so that the cells are the ones in contact with the mounting medium.
      iii. Optional to put a big coverslip on top
   (b) Cultures on **fibrous scaffolds:**

i. Remove the plastic ring
ii. With a forcep, pick up the fiber scaffold and place it onto the glass slide face up (cells up). Perhaps try to remove the excess buffer from the fibers, by touching sideways a paper mat.
iii. Immediately (fast) add a drop of the mounting medium on top of the fiber scaffold, and make sure that it cover all fiber mesh.
iv. Place a cover slip on top of the sample avoiding bubbles

7. Place the glass slides into the carton folder and store it at −20 °C freezer

ALAMAR BLUE ASSAY

Materials and Reagents:

- AlamarBlue kit
- Culture media
- 96 well plate with opaque black walls for fluorescence measurements
- 3 % SDS solution
- Aluminium foil

Procedure:

1. On the day of viability assay, prepare AlamarBlue (AB) solution by mixing 1:9 (1/10th volume) of AlamarBlue:Culture medium. Note: prepare some extra for blank/negative controls
2. Aspirate all culture medium from each culture well and immediately add 400 µl (if using a 24w plate) of freshly prepared AB solution
3. Wrap the plates with aluminium foil (protection from direct light)
4. Incubate at 37 °C. Determine the time of incubation by checking the plate every hour
5. Add 50 µl of 3 % SDS solution into each well to wells in a 96w plate (black walls). Note: only the number of wells necessary)
6. Transfer 100 µl from each well of the medium after incubation with AB solution to individual wells in a 96w plate containing 3 % SDS. SDS will stop the reaction.
   NOTE: Plate can be stored at RT for up to 24hrs (or 1 d to 3 d at 4 °C) before recording data, provided that the contents are protected from light and covered to prevent evaporation.
7. Record results using fluorescence or absorbance as follows:
   - Fluorescence measured at 530-570 nm excitation wavelength and 590nm (580-620nm) emission wavelength
   - Absorbance is monitored at 570 nm and 600 nm